GROWTH OF FERRO-ELECTRIC TUNGSTEN BRONZE EPITAXIAL THIN FILMS FOR ELECTRO-OPTIC DEVICE APPLICATIONS

Final Technical Report
For Period 09/30/82 through 11/30/85

JUNE 1986

DARPA Order No.:	4540
Program Code:	P2D10
Name of Contractor:	Rockwell International Corporation
Effective Date of Contract:	9/30/82
Contract Expiration Date:	11/30/85
Contract Number:	N00014-82-C-2466
Principal Investigators:	Dr. R.R. Neurgaonkar (805) 373-4109
	Dr. L.E. Cross Pennsylvania State University (814) 856-1181

Sponsored by

Defense Advanced Research Projects Agency (DoD)
DARPA Order No. 4540

Monitored by Naval Research Laboratory
Under Contract No. N00014-82-C-2466

The views and conclusions contained in this document are those of the authors and should not be interpreted as necessarily representing the official policies, either expressed or implied, of the Defense Advanced Research Projects Agency of the U.S. Government.

Approved for public release; distribution unlimited

UNCLASSIFIED
SECURITY CLASSIFICATION OF THIS PAGE

AD-A170 783

REPORT DOCUMENTATION PAGE

1a. REPORT SECURITY CLASSIFICATION Unclassified	1b. RESTRICTIVE MARKINGS
2a. SECURITY CLASSIFICATION AUTHORITY	3. DISTRIBUTION/AVAILABILITY OF REPORT Approved for public release; distribution unlimited.
2b. DECLASSIFICATION/DOWNGRADING SCHEDULE	
4. PERFORMING ORGANIZATION REPORT NUMBER(S) SC5340.13FR	5. MONITORING ORGANIZATION REPORT NUMBER(S) Code 6822
6a. NAME OF PERFORMING ORGANIZATION Rockwell International Science Center 6b. OFFICE SYMBOL (If applicable)	7a. NAME OF MONITORING ORGANIZATION Naval Research Laboratory
6c. ADDRESS (City, State and ZIP Code) 1049 Camino Dos Rios Thousand Oaks, CA 91360	7b. ADDRESS (City, State and ZIP Code) 4555 Overlook Avenue S.W. Washington, D.C. 20375
8a. NAME OF FUNDING/SPONSORING ORGANIZATION Defense Advanced Research Projects Agency (DoD) 8b. OFFICE SYMBOL (If applicable)	9. PROCUREMENT INSTRUMENT IDENTIFICATION NUMBER Contract No. N00014-82-C-2466
8c. ADDRESS (City, State and ZIP Code)	10. SOURCE OF FUNDING NOS. PROGRAM ELEMENT NO. / PROJECT NO. DARPA ORDER NO. 4540 / TASK NO. / WORK UNIT NO.
11. TITLE (Include Security Classification) GROWTH OF FERRO-ELECTRIC TUNGSTEN BRONZE EPITAXIAL THIN FILMS FOR ELECTRO-OPTIC DEVICE APPLICATIONS (U)	
12. PERSONAL AUTHOR(S) Neurgaonkar, R.R. and Oliver, J.R.	
13a. TYPE OF REPORT Final Technical Report 13b. TIME COVERED FROM 09/30/82 TO 11/30/85	14. DATE OF REPORT (Yr., Mo., Day) JUNE 1986 15. PAGE COUNT 63
16. SUPPLEMENTARY NOTATION The views and conclusions contained in this document are those of the authors and should not be interpreted as necessarily representing the official policies, either expressed or implied, of the Defense Advanced Research Projects Agency or the U.S. Government.	
17. COSATI CODES FIELD / GROUP / SUB GR.	18. SUBJECT TERMS (Continue on reverse if necessary and identify by block number) SBN, PBN, Doped-SBN:60, LPE Growth, Tungsten Bronze, Photorefractive speed and sensitivity, striations

19. ABSTRACT (Continue on reverse if necessary and identify by block number)

SBN:60 doped with Ce^{+} and Fe crystals have now been grown with improved optical quality using the Czochralski technique. The liquid phase epitaxial(LPE) growth of SBN:46 on SBN:60 substrate has also been successfully demonstrated, with particularly good results for (100) and (110) film orientations.

The recent photorefractive measurements on Ce-doped SBN:60 crystals show that the T. B. SBN:60 crystals are superior in many respects to $BaTiO_3$ because of enhanced two-beam coupling coefficients, sensitivity and the overall flexibility of tungsten bronze crystals.

$La^{(3+)}$-doped SBN:50 single crystals have also been grown for pyroelectric detector studies and it was found that the growth of doped crystals is possible. Crystals as large as 1 to 1.5 cm in diameter have been grown successfully. Current measurements show that this composition exhibits excellent pyroelectric and dielectric properties to use —

20. DISTRIBUTION/AVAILABILITY OF ABSTRACT UNCLASSIFIED/UNLIMITED ☐ SAME AS RPT. ☒ DTIC USERS ☐	21. ABSTRACT SECURITY CLASSIFICATION Unclassified
22a. NAME OF RESPONSIBLE INDIVIDUAL	22b. TELEPHONE NUMBER (Include Area Code) 22c. OFFICE SYMBOL

DD FORM 1473, 83 APR EDITION OF 1 JAN 73 IS OBSOLETE.

UNCLASSIFIED
SECURITY CLASSIFICATION OF THIS PAGE

in longitudinal configuration; hence, work is in progress to use this composition for pyroelectric detector applications. The role of other cations such as calcium and yttrium has also been studied and they appear to be promising for the proposed device applications.

TABLE OF CONTENTS

LIST OF FIGURES

LIST OF FIGURES

LIST OF TABLES

1.0 SUMMARY AND PROGRESS

The tungsten bronze (T.B.) crystal family has been shown to be useful for a variety of device applications, including electro-optic, photorefractive, pyroelectric and many others. The current work reports on the development of good quality (acceptable for proposed device studies) $Sr_{1-x}Ba_xNb_2O_6$, where x = 0.40 and 0.50, and morphotropic phase boundary (MPB) compositions. Several MPB systems have been identified in the present work and some of these compositions are exceedingly useful for optical and nonlinear optical applications. Considerable progress has been made in several areas, including the growth of Ce- and Fe-doped SBN:60, La-doped SBN:50, and PBN:60 (at Penn State) crystals and the characterization of their ferroelectric, electro-optic and photorefractive properties. Based on current work, a number of new dopants have been proposed for future photorefractive and pyroelectric device studies.

Several doped (Ce^{3+}/Ce^{4+}, Fe^{2+}/Fe^{3+} and Ce^{3+}/Fe^{3+}) and undoped SBN:60 single crystals have been grown by the Czochralski technique, and crystals as large as 2 to 2.5 cm in diameter have been routinely grown. The speed or rate per unit intensity for a 0.1 wt% Ce-doped SBN:60 crystal is estimated to be 1 $cm^2/W\text{-}s$. Charge density measurements on undoped and Ce-doped SBN:60 crystals indicate that the charge increases from 2.4×10^{15} to 5.4×10^{16} cm^{-3} going from undoped to doped crystals, indicating that the enhancement in response time is connected to the presence of Ce in the crystal. However, the concentration of Ce appears to be lower than needed to get optimum charge density for this composition. It is expected that by increasing the Ce concentration, it may be possible to increase both the charge density as well as response speed for this crystal. Therefore, further work will include the determination of the optimum Ce concentration and we also plan to introduce other dopants such as Mn, Cr and Nd.

La^{3+}-doped SBN:50 single crystals have also been grown for pyroelectric detector studies and it was found that the growth of doped crystals is easier than that for undoped SBN:50 crystals. Crystals as large as 1 to

1.5 cm in diameter have been grown successfully. Current measurements show that this composition exhibits excellent pyroelectric and dielectric properties; hence, work is in progress to use this composition for pyroelectric detector applications. The role of other cations such as Ca^{2+} and Y^{3+} has also been studied and they appear to be promising for the proposed device applications.

The results of theoretical and experimental studies of the photorefractive effect in two different classes of materials such as perovskite $BaTiO_3$ and tungsten bronze SBN crystals have been examined. The interesting features of these measurements indicate that the two-beam coupling coefficients, response time and absorption coefficients are enhanced significantly for doped crystals and they appear to be suitable for future device concepts. The comparison of these measurements shows that Ce-doped SBN:60 single crystals are superior in many respects to $BaTiO_3$ because of enhanced two-beam coupling coefficients, sensitivity and the overall flexibility of tungsten bronze crystals.

This report also documents preliminary results of the epitaxial growth of tetragonal ferroelectric SBN thin films by the liquid phase epitaxial (LPE) technique. Several V^{5+}-containing flux systems were investigated. However, the BaV_2O_6 flux was found to be most efficient in producing SBN solid solution films. Although the film growth rate was much faster on the <100> direction, film quality was best on the <100> and <110> directions with thicknesses in the range of 5-20 μm. Lattice constant measurements indicate that the films are Ba^{2+}-rich, with compositions close to $Sr_{0.46}Ba_{0.54}Nb_2O_6$ and $Sr_{0.4}Ba_{0.6}Nb_2O_6$. This technique offers a unique opportunity to develop simple or complex bronze films of superior quality for several optoelectronic device applications.

2.0 DEVELOPMENT OF OPTICAL QUALITY SBN CRYSTALS

2.1 Material Growth Techniques

Most of the bronze compositions grown in our laboratory are based on solid solution systems; therefore, suitable growth techniques to produce crystals free of optical defects such as striations, scattering centers and twinning must be developed. Striations and other defects are typical problems common to solid solution crystals, and it is often difficult to suppress them completely. However, these problems can be reduced effectively such that the crystals can be useful for optical device studies. The difficulty of this task underscores the criticality of selecting appropriate growth techniques in the present work. At present, three different techniques have been chosen to develop SBN and other bronze crystals. They are as follows:

1. Bulk Single Crystals: Czochralski technique

2. Thin Films: Liquid phase epitaxy (LPE)

3. Strip Crystals: Edge-defined film-fed technique

The first two techniques are well established in our current work, and bulk crystals and films of SBN compositions have already been grown. In the present report, the continued growth of striation-free SBN crystals is discussed along with associated growth problems.

2.2 Growth Procedure

Nb_2O_5, $SrCO_3$, CeO_2 and $BaCO_3$ fine powders have been used as starting materials and have been weighed out in the desired proportions, as summarized in Table 1. The batch mixture is ball-milled in acetone for 20-30 h, and then poured into a large drying dish. The dried powder is placed in a platinum reaction dish and is calcined at 1000°C for 10-15 h to eliminate carbonates

Table 1
Materials for Bulk Single Crystal SBN:60 Growth

Crystal Composition	Starting Materials		Conditions and Remarks
SBN:60	a. $SrCO_3$	135.08 gms	Congruent melting composition
	b. $BaCO_3$	115.48 gms	Large crystals can be grown
	c. Nb_2O_5	398.73 gms	Large electro-optic coefficient (r_{33})
	Total wt.	649.26 gms	Melts at 1510°C
	Growth wt.	450.00 gms	Crack-free and optical quality
SBN:50 + La^{5+}	a. $SrCO_3$	gms	Dielectric and pyroelectric
	b. $BaCO_3$	gms	coefficient increased
	c. Nb_2O_5	gms	Growth of large crystals is
	d. La_2O_3		possible
		to	Enhanced photorefractive properties
	Total wt.		Crack-free crystals
	Growth wt.	450.00 gms	
SBN:60 + Ce^{3+}	a. $SrCO_3$	135.08 gms	Dielectric and electro-optic
	b. $BaCO_3$	115.48 gms	coefficient improved
	c. Nb_2O_5	398.73 gms	Growth of large crystals is
	d. CeO_2	1.00 gms	possible
		to	Enhanced photorefractive
		1.50 gms	properties
	Total wt.	650.26 gms	Crack-free and optical quality
	Growth wt.	450.00 gms	crystals

and any possible carbon from the pyrolytic breakdown of residual acetone. The calcined powder is then ball milled and refired in an oxygen flow of 2 cfh at 1400°C for about 4-6 h. Phase checks and x-ray lattice constant measurements

are made for each batch to ensure the use of a phase-pure bronze composition for crystal growth. A thick-walled platinum crucible of 2 × 2 in. in dimension is used for this growth, and this container holds roughly 450 g of melt composition.

2.3 Growth of $Sr_{1-x}Ba_xNb_2O_6$, x = 0.40 and 0.50 Crystals

As summarized in Table 2, we have grown a number of doped (Ce, Fe, La, etc.) and undoped SBN:60 and SBN:50 single crystals of excellent quality using the Czochralski technique. Small amounts of impurities have been shown to have a drastic photorefractive effect in optical applications. Based on our current device need, the growth of these compositions has been tailored as follows:

a. Optical Wave Guide and Switches: High-quality starting materials to avoid photorefractive effect and striations. SBN:60 composition has only been used for this task. Required properties of selected crystal:

   1. High electro-optic coefficient.
   2. Optical quality crystals

b. Photorefractive Studies: High optical quality starting materials with specific impurities, e.g., Ce, Fe or both in SBN:60 and possibly in SBN:75 (optimum r_{33}). Required properties in the grown crystals:

   1. High electro-optic coefficient
   2. Fast response time
   3. Large sensitivity
   4. Optical quality crystals

c. Pyroelectric Studies: High optical quality starting materials. Required properties in the grown SBN:50 and SBN:60 crystals are:

1. Large pyroelectric coefficient
2. Moderately large dielectric constant
3. Low dielectric losses (Tan δ)
4. Reasonable crystal quality

As we discussed in our Semi-Annual Report No. 5, we successfully demonstrated the growth of Ce- and Fe-doped SBN:60 single crystals as part of our effort to study in detail the role these ions in photorefractive device applications. Table 2 summarizes the number of crystals grown during the last six months. Doping SBN:60 with Fe, and Fe and Ce together, has not been done previously, and Fe is expected to produce interesting results, as it has been observed to do in other ferroelectric crystals such as $LiNbO_3$ and $KNbO_3$.

Ce-doped SBN:60 single crystals show minumum or no striations, and the crystals are of optical quality, while Fe-doped crystals are highly striated under all growth conditions, and the striations are found difficult to suppress. The development of striation-free Ce-doped SBN:60 single crystals makes possible the evaluation of their photorefractive properties, specifically, speed, sensitivity and coupling coefficients. Typically, 6 × 6 × 6 mm cubes have been supplied for examination, and two- and four-wave mixing techniques are being used. These measurements will be continued as better quality crystals and different dopant levels are used. In agreement with the results reported by Megumi, et al,[1] the present crystals show the typical Ce broad absorption band around 0.50 μm, and this band remains unchanged from one sample to another. Both the photorefractive speed and sensitivity have been estimated and the results of this investigation are given in Table 3. Figure 1 shows the absorption spectra for both the Ce- and Fe-doped SBN:60 crystals.

Table 2

Growth of $Sr_{1-x}Ba_xNb_2O_6$, x = 0.40, 0.50 Crystals

Exp. No.	Date	Boule Wt., gm	Boule size L x ø, cm	Comp. Sr/Ba	Wt. % Dopant	Dip, °C
218	05/07/85	44	2.0 × 1.8	60/40	---	1485
219	05/08,35	39	~ 2 × 2.0	60/40	---	1485
220	05/13/85	14	3.0 × 1.0	50/50	1% La_2O_3	1483
221	05/22/85	18	2.0 × 1.5	50/50	1% La_2O_3	1484
222	05/28/85	38	2.0 × 2.0	60/40	---	1485
223	05/30/85	30	2.0 × ~ 1.6	5/50	1% La_2O_3	1481
224	06/12/85	39	3.0 1.6	60/40	Ce + Mn, 0.004 + 0.001	1485
225	06/17/85	35	2.5 × 1.7	60/40	Ce + Mn, 0.004 + 0.001	1484
226	06/19/85	32	2.0 × 1.9	60/40	Ce + Mn, 0.004 + 0.001	1483
227	07/16/85	19	2.0 × 1.3	50/50	Nb_2O_5, 2 mole % + La	1485
228	07/19/85	17	2.0 × 1.3	50/50	Nb_2O_5, 2 mole % + La	1484
229	07/23/85	19	2.2 × 1.3	50/50	Nb_2O_5, 2 mole % + La	1484
230	07/26/85	18	2.4 × 1.3	60/40	per No. 226	1484
231	08/01/85	25	3.0 × 1.4	60/40	per No. 230	1484
232	08/09/85	39	3.0 × 1.7	60/40	---	1484
233	08/19/85	40	2.5 × 1.7	60/40	---	1484
235	10/01/85	3	1.3 × 0.8	60/40	---	1484
236	10/04/85	11	2.0 × 1.0	60/40	---	1485
237	10/11/85	8	2.0 × 0.9	60/40	---	1485
238	10/22/85	10	2.0 × 0.9	60/40	---	1480
239	10/25/85	12	2.0 × 1.1	60/40	---	1485
240	10/30/85	21	2.0 × 1.2	60/40	0.017 gm CeO_2R	1485
241	11/07/85	15	3.0 × 1.1	60/40	0.017 gm CeO_2R	1485

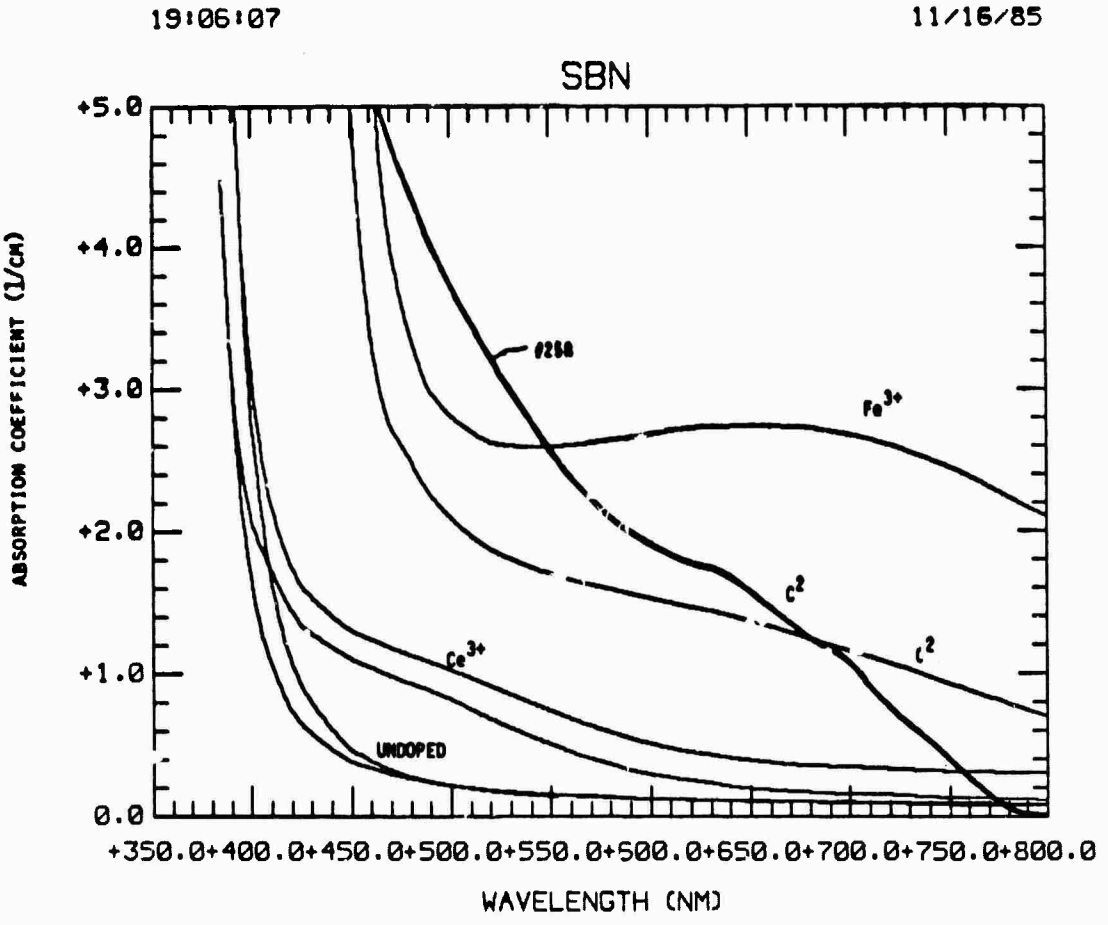

Fig. 1 Absorption spectra for the Ce- and Fe-doped SBN:60 crystals.

Recently, the photorefractive charge density in Ce-doped SBN:60 crystals were also estimated and the results are summarized as follows:

Sample	K_0 (μm^{-1})	n_r (cm^{-3})	Speed (ms)
Undoped SBN:60	2.4	6.4×10^{15}	1000
Ce-doped SBN:60 (0.5 Wt%)	4.4	2.1×10^{15}	--
Ce-doped SBN:60 (0.2 Wt%)	5.4	3.1×10^{16}	80

Table 3

Goals for Photorefractive Studies and Current Results

Desired Properties	Observed Properties
1. Response time ~ 1 ms	1. Response time achieved < 100 ms
2. Sensitivity ~ 10^{-4} to 10^{-5} cm^2/J	2. Sensitivity achieved ~ 10^{-3} cm^2/J
3. Coupling coefficient ~ 1 cm^{-1}	3. Coupling coefficient achieved ~ 11 cm^{-1}
4. Large size, optical quality crystals	4. Large size (2.5 cm in diameter) and striation-free SBN:60 and Ce^{3+}-doped SBN:60 crystals are available
5. Large electro-optic coefficient necessary	5. Electro-optic coefficient enhanced for Fe^{3+} and Ce^{3+} additions

It is clear from these measurements that the charge density increases as the Ce concentration in SBN:60 is increased. However, this value has not saturated with respect to Ce concentration. To improve the response time without adversely affecting the sensitivity, it appears that the addition of more Ce in SBN:60 should be advantageous. During the next six months, effort will be extended to further increase the Ce concentration to obtain an optimum response time. We also plan to explore the effects of other dopants, individually or together with Ce, as follows:

	Proposed Crystallographic Sites	
Cation	15- or 12-fold	6-fold
Ce + Fe	Ce^{3+}	Fe^{3+}
Ce + Cr	Ce^{3+}	Cr^{3+}
Cr + Fe	--	Fe^{3+} + Cr^{3+}
Nd + Fe	Nd^{3+}	Fe^{3+}
Ce + Nd	Ce^{3+}, Nd^{3+}	--

Initially, all the substitutional dopant work will be carried out using sintered ceramic disks, and their ferroelectric properties, specifically the Curie temperature, dielectric constant and dielectric losses, will be established. Since the dielectric constant is directly proportional to electro-optic coefficient, samples exhibiting large dielectric constants will be selected for further crystal growth study.

Currently, efforts are underway at our laboratory as well as at Caltech to establish the valence states of Ce in SBN:60 single crystals. It is believed that for efficient performance, one needs the presence of both Ce^{3+} and Ce^{4+} states in the crystals. However, from the current results, the proportion of these states in SBN:60 is not clear. The enhancement of the sensitivity and speed indicate that there may be other impurities such as Nb^{4+} or Fe^{3+} present in the crystals. Measurements such as x-ray fluorescence and Mossbauer could be effective in identifying these impurity levels and their valence states.

2.4 T.B. Crystals for Pyroelectric Detectors

There is a need for reliable, mass producible and low-cost IR imaging systems for medium performance tactical applications. These systems include thermal sights, short-range missile seekers and smart munitions. Uncooled IR imagers offer major advantages over cryogenically cooled imagers due to the elimination of refrigerators or thermoelectric coolers; this results in weight savings, reduced power consumption and lower costs. Substantial improvement in systems reliability and field maintainability are also expected.

Ferroelectric IR detectors use the pyroelectric effect inherent in these materials. The absorbed radiation raises the temperature of the detector element, changing its polarization. The detector, made in the form of a capacitor, develops a transient voltage drop across its terminals proportional to its temperature change. The detector can be operated below the ferroelectric phase transition with the material spontaneously poled, or it can be operated in the vicinity of the phase transition temperature, in which case

the polarization is maintained by an external bias. The latter mode offers higher power conversion efficiency, although lower voltage responsitivity, than the former mode of operation. In either case, operation at room temperature can be achieved with many material compositions.

At Rockwell, two different configurations, namely transverse and longitudinal, are being explored to obtain optimum pyroelectric response for IR detector applications. Figure 2 shows the polar direction in each configuration. The figure-of-merit in each case is p/ε, where p is the pyroelectric coefficient. However, the conditions established for each configuration are different and they are as follows:

Longitudinal	Transverse
* Figure-of-Merit, p/ε	* Figure-of-Merit, p/ε
* Large pyroelectric coefficient (p)	* Large pyroelectric coefficient (p)
* Low tan δ at operating frequency	* Low tan δ at operating frequency
* Low dielectric constant (ε)	* High dielectric constant with high p/ε

There are a number of ferroelectric materials that exhibit an excellent pyroelectric figure-of-merit (Table 4). However, the tungsten bronze family compositions appear to be more suitable for this study because of their versatility and ease of fabrication.

Since the SBN:50 single crystals exhibit excellent pyroelectric figures-of-merit, efforts are underway in our laboratory to build IR detectors using these crystals. Although the size and performance of these crystals appear to be reasonable, there is always room for improvement of the pyroelectric response. The improvement in response, that is, the enhancement of p/ε, in a given crystal or family can be attempted in several ways:

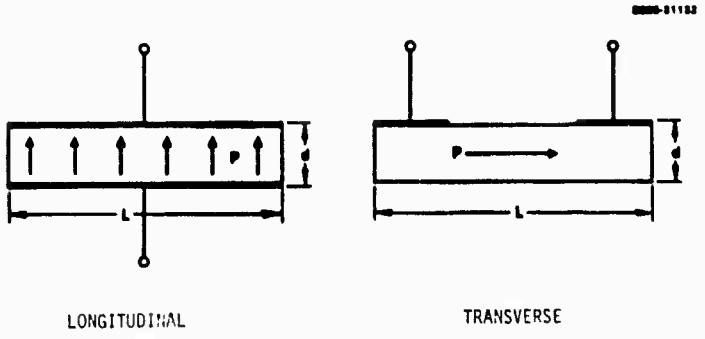

Fig. 2 Longitudinal and transverse detector configuration.

1. Alter the host composition, i.e., use a host exhibiting better pyroelectric properties than the current SBN:50 or SBN:60.

2. Establish crystal chemical control in SBN:50, i.e., the use of dopants to enhance the pyroelectric coefficient.

3. Use of tilted cuts, i.e., orient the crystal in different directions to find the optimum pyroelectric properties.

In the present work, we plan to explore some of these approaches. However, during the last six months, we have studied the crystal chemical approach to enhance the pyroelectric response for SBN:50. The recent work by Liu, et al[2] showed that the pyroelectric coefficient of SBN:50 is increased from 600 to 3700 $\mu coul/m^2$-°C for the addition 1.5 wt% La^{3+}. This is a significant improvement for this crystal and it is our intention to continue this work in more detail, and to also study the role of other cations such as Ca^{2+} and Y^{3+} in SBN:50. Table 5 summarizes the site preferences, the Curie temperature and dielectric properties for these different cation additions.

Table 4

Leading Pyroelectric Materials

Crystal Composition	T_c (°C)	Dielectric Constant at 23°C	Pyroelectric Coefficient $\times 10^{-10}$ c/cm^{-2} K^{-1}	Figure-of-Merit P/ε	Figure-of-Merit $P/\sqrt{\varepsilon}$
TGS	49	28	310	11.07	58.58
TGS:P^{4+}*	50	-	-	-	-
$LiTaO_3$	660	49	170	3.47	24.28
SBN:60	75	500	850	1.82	38.01
SBN:50	128	300	680	2.28	39.26
SBN:50, 0.5%La^{3+}	106	485	1562	3.22	70.92
BSKNN	208	120	485	4.04	44.27
$Pb_5Ge_3O_{11}$	152	36	110	3.065	18.33

*Work is in progress to obtain optimum dopant concentration.

Table 5

Proposed Site Preferences for Various Cations in SBN

Ion	Ionic Radius (Å)	Crystallographic Site Preference 15-Fold	12-Fold	9-Fold
Ba^{2+}	1.74	Ba^{2+}	Ba^{2+}	--
Sr^{2+}	1.54	Sr^{2+}	Sr^{2+}	--
Ca^{2+}	1.40	--	Ca^{2+}	--
La^{3+}	1.46	La^{3+}	La^{3+}	La^{3+}
Y^{3+}	1.15	--	--	Y^{3+}

2.4.1 The Role of Ca^{2+} in SBN:50

Ca^{2+} (1.14Å) is much smaller than both Sr^{2+} (1.27Å) and Ba^{2+} (1.50Å) cations, and its location in the tungsten bronze structure is not well understood. According to work reported by Ainger, et al[3] and Ikeda, et al,[4] it appears that Ca^{2+} is on both the 15- and 12-fold coordinated sites. However, there is not sufficient data to substantiate these results. Based on our current work on Ca^{2+} substitution in SBN:50 and our unpublished work on the $Sr_2NaNb_5O_{15}$-$Ca_2NaNb_5O_{15}$ system, we have found that the solubility of Ca^{2+} is about 30 mole%, which is equivalent to two atoms in $(A_1)_4(A_2)_2B_{10}O_{30}$. Beyond this limit, two phases have been identified, indicating that the substitution of Ca^{2+} in the 15-fold coordinated site is difficult. Although further work is necessary to identify the site preference of Ca^{2+} in the tungsten bronze structure, it appears that Ca^{2+} prefers the 12-fold coordinated site. The substitution of Ca^{2+} in SBN:50 has been made in the following two ways:

1. $Sr_{0.5-x}Ca_xBa_{0.5}Nb_2O_6$

2. $Sr_{0.5}Ba_{0.5-x}Ca_xNb_2O_6$

The present substitutions can be represented on a ternary diagram as $SrNb_2O_6$-$CaNb_2O_6$-$BaNb_2O_6$. A considerable amount of work has been performed to the limit of the solid solubility range of the various phases existing in this diagram. However, the T.B. orthorhombic and tetragonal phases exist over a wide compositional region, as compared to other phases.

As shown in Fig. 3, it is observed that although Ca^{2+} is considered to be only on the 12-fold coordinated site, its effect on the 1 and 2 compositions is entirely different. For example, the Curie temperature is slightly increased when Sr^{2+} is replaced by Ca^{2+} in $Sr_{0.5-x}Ca_xBa_{0.5}Nb_2O_6$, whereas in the composition $Sr_{0.5}Ba_{0.5-x}Ca_xNb_2O_6$ the Curie temperature is reduced significantly. This is the first time such data has been recorded for this composition, and further ferroelectric characterization of these compositions will be

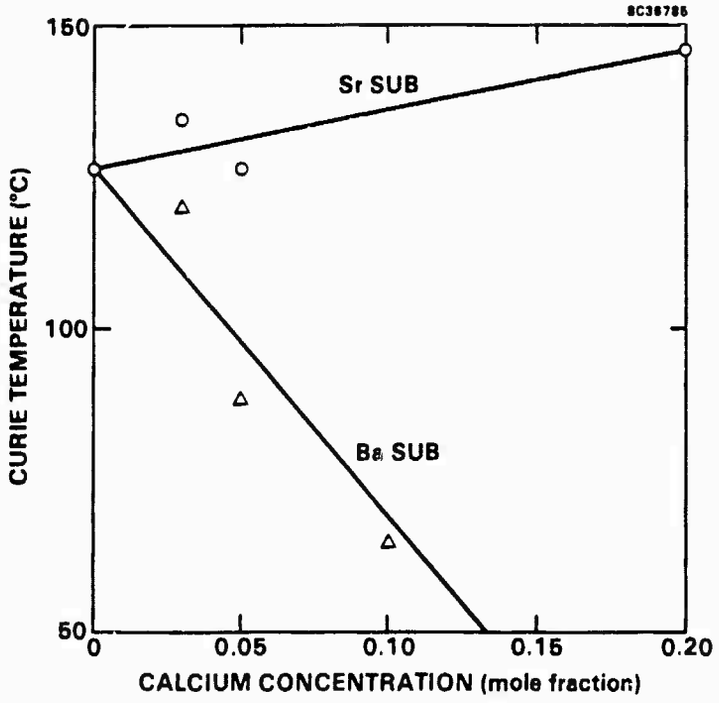

Fig. 3 Curie temperature for $Sr_{0.5-x}Ca_xNb_2O_6$ and $Sr_{0.5}Ba_{0.5-x}Ca_xNb_2O_6$.

performed to distinguish this behavior and also to confirm the location of Ca^{2+} in the tungsten bronze structure.

The room temperature dielectric constants for both systems have been measured and they increase significantly with increasing Ca^{2+}, reaching a maximum of 2000 for the $Sr_{0.50}Ba_{0.30}Ca_{0.20}Nb_2O_6$ composition. This value is almost five times larger than for undoped SBN:50. For a transverse pyroelectric detector, one needs such a large dielectric constant; hence, we believe this composition could have a significant impact. Once the phase relation and congruent melting behavior for this system is studied, effort will then be made to grow small size crystals for pyroelectric detector evaluation.

2.4.2 The Role of La^{3+} and Y^{3+} in SBN:50

The substitution of La^{3+} and Y^{3+} in SBN:50 has been made in the following two ways:

1. $Sr_{0.5-x}M_x^{3+}Ba_{0.5}Nb_2O_6$

2. $Sr_{0.5-3x}M_{2x}^{3+}Ba_{0.5}Nb_2O_6$

The ionic size of La^{3+} (1.40Å) is similar to Sr^{2+} and it is expected that this ion should occupy both the 15- and 12-fold coordinated sites. Y^{3+} (1.04Å) is comparatively smaller than Sr^{2+}; hence, we expect Y^{3+} to occupy either the 12- or 9-fold coordinated sites. The solid solubility of these ions has been studied only up to 8 mole%, and for this addition, we have observed a single phase. Although the site preference for thse ions has not yet been established, the Curie temperature is reduced for all additions of La^{3+} and Y^{3+}.

The dielectric constant for these additions has been determined as a function of concentration. Figures 4 and 5 show the dielectric behavior with

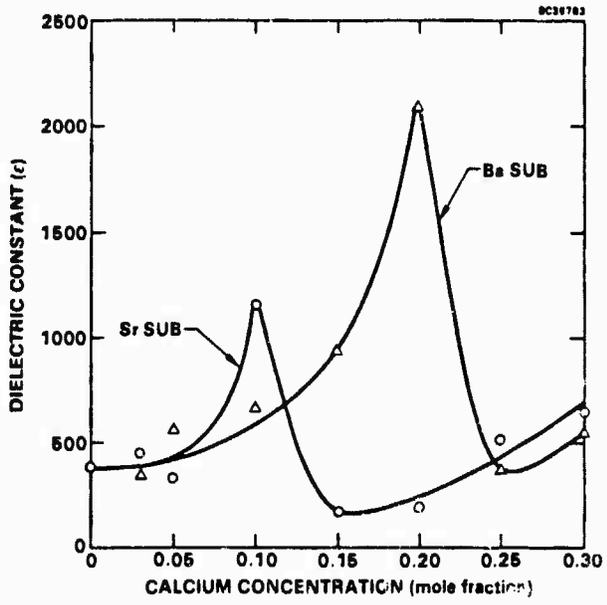

Fig. 4 Room temperature dielectric constant for $Sr_{0.5-x}Ca_xNb_2O_6$ and $Sr_{0.5}Ba_{0.5-x}Ca_xNb_2O_6$ systems.

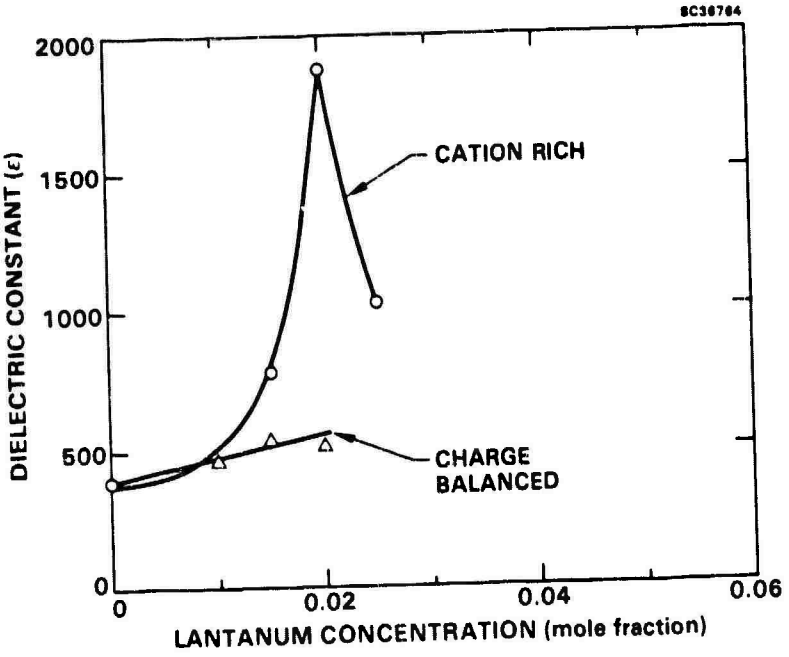

Fig. 5 Room temperature dielectric constant for $Sr_{0.5-x}La_xBa_{0.5}Nb_2O_6$ and $Sr_{0.5-3x}La_{0.2x}Ba_{0.5}Nb_2O_6$ systems.

respect to La^{3+} and Y^{3+} in two different compositions. From these results, it is clear that when one Sr^{2+} is replaced by one La^{3+} (composition 1), the increase in the dielectric constant is significantly greater than when three Sr^{2+} are replaced by two La^{3+} in the second composition. A similar behavior is also observed for the Y^{3+}-doped SBN:50 compositions. The highest room temperature dielectric constants for these two different systems were 2000 for La^{3+} and about 4000 for Y^{3+} substituted compositions. These values are 5-9 times larger than for undoped SBN:50. This significiant increase indicates that by using proper dopants at appropriate concentrations, it should be possible to control both the pyroelectric coefficient and the dielectric constant required for thermal detectors. The results are very promising and further efforts will be made to study in detail the role of these ions. La^{3+}-doped SBN:50 crystals have now been grown and the results of this work are summarized in the next section.

2.4.3 Growth of La^{3+}-doped SBN:50 Crystals

Undoped SBN:50 single crystals were originally grown in the present work for use as substrate material for the liquid phase epitaxy (LPE) growth of bronze compositions. Since SBN:50 exhibits a large pyroelectric coefficient, and since the Curie temperature for this crystal is over 125°C, it is important that this crystal be further developed. However, growth is more difficult than the congruent melting composition, SBN:60, due to cracking. In our earlier experiments, SBN:50 crystals were grown using an automatic diameter control system, and small crystals of ~ 1 cm in diameter were successfully grown. Although these crystals showed a tendency to crack, their dielectric properties were reasonable. To suppress the cracking problem and also to enhance the pyroelectric figure-of-merit, about 1 mole% La^{3+} was added. The addition of La^{3+} slightly reduced the growth temperature (5°C), and this helped to further suppress crystal cracking. As shown in Fig. 6, crystals ~ 1-1.5 cm in diameter have been grown, and further efforts are underway to perfect the growth parameters for this composition. According to our current crystal chemistry work, about 2% La^{3+} is needed to obtain optimum pyroelectric and dielectric properties. At present, La^{3+}-doped SBN:50 crystals are being evaluated for their structural and ferroelectric properties, and based on these findings, we will increase the La^{3+} content accordingly.

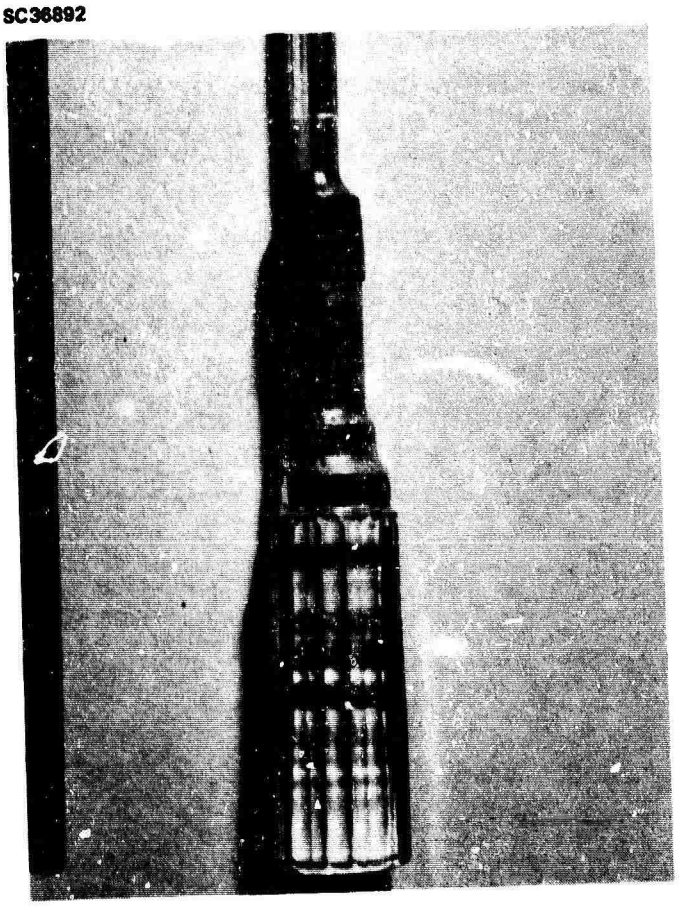

Fig. 6 Typical La^{3+}-doped SBN:50 single crystal grown along the (001) direction.

3.0 PHOTOREFRACTIVE PROPERTIES OF FERROELECTRIC $BaTiO_3$ and SBN:60

3.1 Introduction

A given photorefractive material is considered useful for optical processing applications, such as phase conjugate optics, if it possesses three important features: low response time, a large coupling coefficient and high optical quality. Speed is necessary if the crystal is to be used in real-time applications, while large photorefractive coupling is required for the construction of efficient devices. However, a crystal of poor optical quality is of little practical importance, regardless of its speed and gain. Although a material has yet to be found which completely satisfies all three requirements, we will show how well $BaTiO_3$, SBN:60, and SBN:60/Ce approximate these properties.

3.2 Material Properties

Strontium barium niobate (SBN) belongs to a class of tungsten bronze ferroelectrics which is pulled from a solid solution of alkaline earth niobates. The crystal is transparent and can be grown with a variety of ferroelectric and electro-optic properties depending on the specific cation ratio introduced into the structure. In SBN, the unit cell contains ten NbO_6 octahedra with only five alkaline earth cations to fill ten interstitial sites. The structure is thus incompletely filled, thereby permitting the addition of a wide range of dopants into the host crystal.

The point group symmetry of SBN at room temperature is 4 mm, which implies that its electro-optic tensor is nonzero. The dominant electro-optic coefficient is r_{33}, which ranges from 100 pm/V in SBN:25 to 1400 pm/V in SBN:75. SBN:75 would, therefore, appear to be the best photorefractive SBN crystal were it not for the fact that optical quality diminishes with increasing Sr concentration beyond SBN:60. Hence, SBN:60 was selected as the candidate SBN photorefractive material on the basis of its high optical quality and moderately large electro-optic coefficient.

Barium titanate has a prototype cubic perovskite structure above 120°C. It successively transforms to three ferroelectric phases below 120°C: first to 4 mm tetragonal, then to mm2 orthorhombic at 5°C, and finally to a 3 m trigonal phase below -90°C. Although $BaTiO_3$ has the same point group symmetry at room temperature as SBN:60, its largest electro-optic coefficient is r_{42}, whose value is ~ 1600 pm/V, rather than r_{33}. This means that in $BaTiO_3$, any intensity variations whose grating vectors are parallel to a crystal axis will not result in refractive index modulation. To obtain the large values of electro-optic coefficients in these crystals, they must, in practice, be poled by first heating them above their Curie points and then allowing them to cool to room temperature with an applied dc electric field on the order of 1-10 kV/cm. It has been observed that SBN:60 is significiantly easier to pole than $BaTiO_3$, since the latter crystal will often be permanently damaged as its temperature approaches its Curie point or if an excessive electric field is applied. SBN:60 crystals, on the other hand, can easily sustain fields up to 10 kV/cm and its temperature can be varied to practically any temperature at moderate rates without fear of damaging the crystal.

3.3 Photorefractive Properties

Single crystals of SBN:60 and SBN:60/Ce grown at Rockwell International, and $BaTiO_3$ obtained from Sanders Associates, Inc. were studied using the two-wave mixing experiment shown in Fig. 7 to determine their effectiveness as photorefractive media. In Fig. 7, beams 1 and 2 are plane waves which intersect in the crystal and thus form an intensity interference pattern. Charge is excited by this periodic intensity distribution into the conduction band, where it migrates under the influence of diffusion and drift in the internal electric field, and then preferentially recombines with traps in regions of low irradiance. A periodic space charge is thus created which modulates the refractive index via the electro-optic effect. This index grating, being out of phase with the intensity distribution, introduces an asymmetry that allows one beam to be amplified by constructive interference with light scattered by the grating, while the other beam is attenuated by destructive

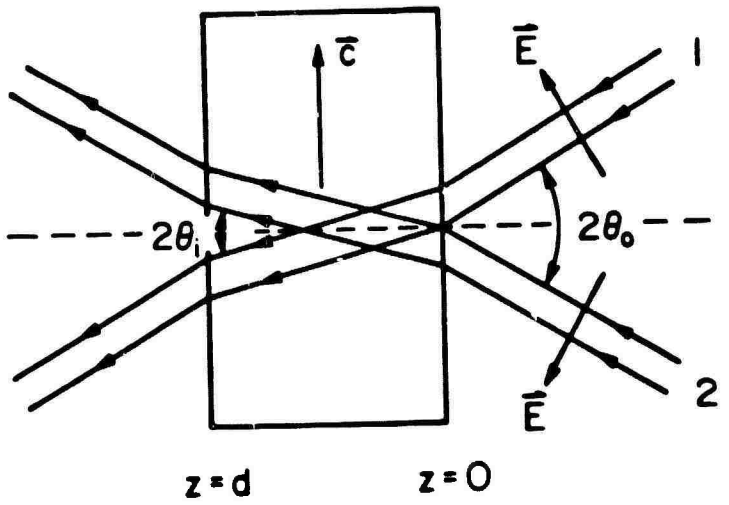

Fig. 7 Two-wave mixing experimental technique.

interference with diffracted light. This process is shown graphically in Fig. 8.

Mathematically, this two-beam coupling may be described in the steady-state as follows:

$$\cos\theta_1 \frac{dI_1}{dz} = \Gamma \frac{I_1 I_2}{I_1 + I_2} - \alpha I_1$$

$$\cos\theta_2 \frac{dI_2}{dz} = -\Gamma \frac{I_1 I_2}{I_1 + I_2} - \alpha I_2 \qquad (3.1)$$

where I_1, I_2 are the intensities of beams 1 and 2 inside the crystal, respectively, Γ is the two-beam coupling coefficient, and α is the absorption coefficient. The transient behavior is modeled by the following:

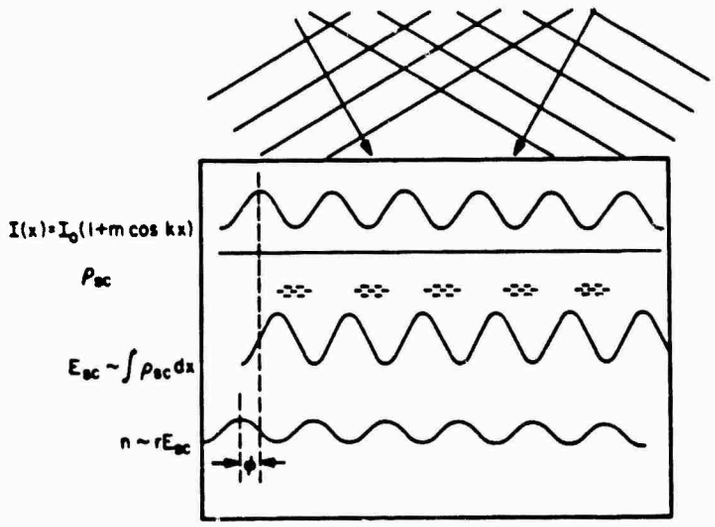

Fig. 8 Photorefractive mechanism

$$I_i(\tau,t) = (1 - e^{-t/\tau})I_i(z,t \to \infty) + e^{-t/\tau}I_i(z,t = 0),\ i = 1,2 \tag{3.2}$$

where τ is a characteristic time constant and

$$I_i(z,t \to \infty) \equiv I_i(z) \ . \tag{3.3}$$

By measuring the four intensities $I_1(0)$, $I_2(0)$, $I_1(d)$, and $I_2(d)$, both in the steady-state and as a function of time, the two-beam coupling coefficient Γ and the response time τ can be obtained from the above equations.

Figures 9, 10, and 11 show the absorption spectra of SBN:60, SBN:60/Ce and $BaTiO_3$, respectively. Several interesting observations can be made. For one, the band edge shifts from 400 nm in SBN:60 to 430 nm in

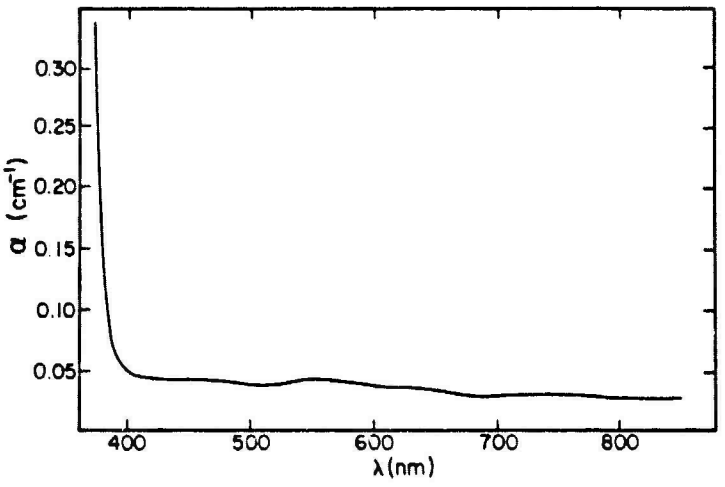

Fig. 9 Absorption spectra of SBN:60.

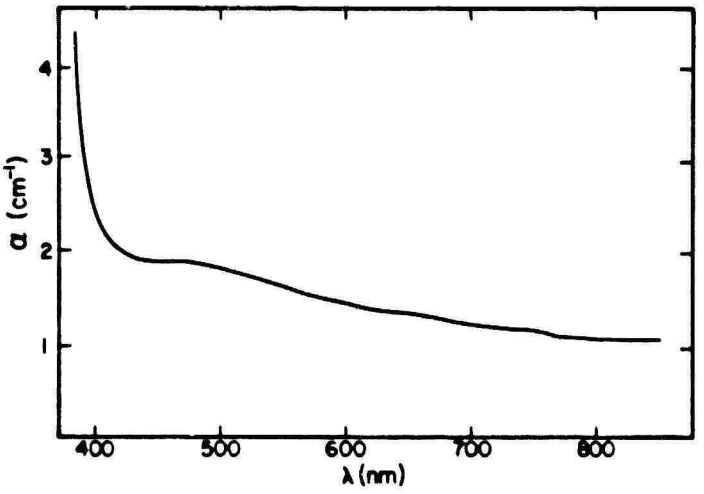

Fig. 10 Absorption spectra of Ge-doped SBN:60.

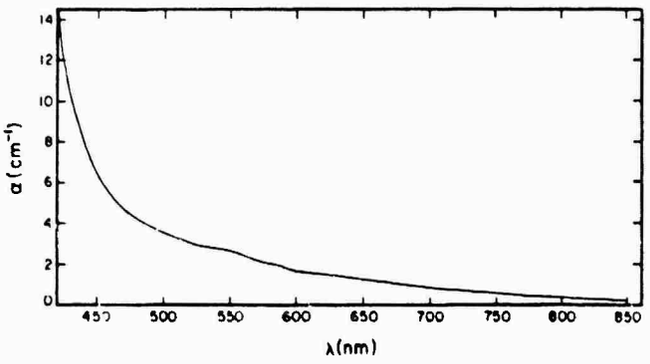

Fig. 11 Absorption spectra of $BaTiO_3$.

SBN:60/Ce, whereas in $BaTiO_3$ a distinct band edge is not identifiable due to, presumably, the presence of a large Urbach tail. Secondly, although the SBN:60 sample was not intentionally doped, there are signs of deep level impurities evidenced by perturbations in the spectrum near 550 nm. In the spectrum of $BaTiO_3$ near 550 nm, and to a lesser extent, near 620 nm, similar observations can also be made. Finally, from Fig. 10, it is seen that the addition of cerium in SBN results in a crystal with a spectrum that is rather featureless with a broad deep level centered at 480 nm.

First principle calculations using the band transport model can be used to derive expressions for Γ and τ. Solutions to the photorefractive equations developed most fully by Kukhtarve show that Γ and τ can be represented functionally as follows:

$$\Gamma = \Gamma(k_g, E_o, \lambda, T; r, N_D, N_A, \varepsilon, n) \qquad (3.4)$$

$$\tau = \tau(k_g, E_o, \lambda, T, I_o; s, \gamma_R) \qquad (3.5)$$

where the experimentally-controlled variables are

k_g = grating wave number
E_o = applied field
λ = wavelength of incident light
T = temperature
I_o = total irradiance

while the material parameters are

r = effective electro-optic coefficient
s = photoionization cross section
γ_R = two-body recombination rate
μ = mobility
N_D = number of donors under dark conditions
N_A = number of traps under dark conditions
ε = static dielectric constant
n = background refractive index

These equations were applied to cerium-doped SBN (10^{18} cm^{-3} Ce atoms) and the theoretical results obtained are displayed in Figs. 12-14.

Figure 12 gives the actual response times as a function of grating wavelength for the three crystals along with the theoretical curve for SBN: 60/Ce, while Fig. 13 displays the corresponding two-beam coupling coefficients. Although $BaTiO_3$ is currently the fastest material of the three, it is significantly less photorefractive than SBN:60/Ce. Therefore, a method was sought for SBN:60/Ce in which the coupling strength could be traded for speed to produce a crystal with a 1 ms response time at 1 W/cm^2 irradiance while still keeping Γ greater than 1 cm^{-1}.

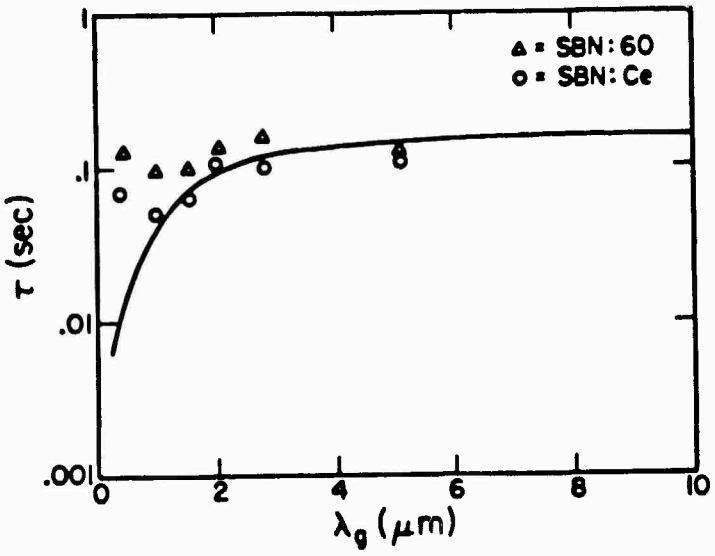

Fig. 12 Response time vs grating wavelength at I_o = 1 W/cm^2 for E_o = 0 V/cm.

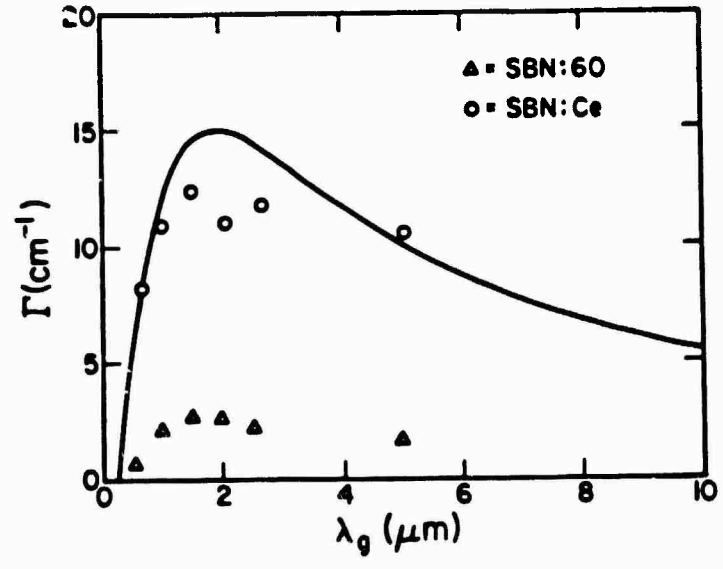

Fig. 13 Coupling coefficient vs grating wavelength for E_o = 0 V/cm.

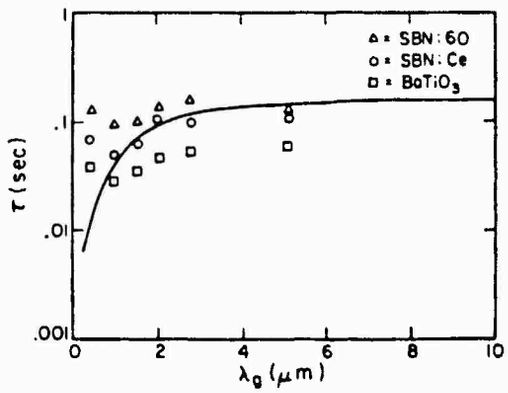

Fig. 14 Response time vs grating wavelength I_0 = 1 W/cm^2 and λ = 0.5145 m.

Such a scheme was proposed in $BaTiO_3$, which suggested that Γ and τ could be modified as indicated in Figs. 13 and 14 by varying the trap density N_A through reduction and oxidation treatments. In principle, if N_A could be reduced from its current value in SBN:60/Ce of 10^{16} cm^{-3} to 5×10^{14} cm^{-3}, the crystal would then possess a coupling coefficient of 2 cm^{-1} with a response time of only 0.001 s. Therefore, an effort was undertaken in which the SBN:60/Ce sample was heated to temperatures ranging from 300°C to 800°C for various lengths of time in atmospheres of differing oxygen partial pressures, and then quickly cooled to room temperature. Then the crystal would be repoled, its absorption spectrum taken, and finally, its photorefractive properties measured.

After performing this exercise many times, we first observed that the SBN:60/Ce crystal was never irreversibly damaged by this treatment, a significant result since $BaTiO_3$ would often crack when subjected to the same process. Secondly, we were able to show that the two-beam coupling coefficient can be

controlled with the heat treatment technique. In fact, values of Γ ranging from less than 0.1 cm^{-1} to 15 cm^{-1} were measured in treated SBN:60/Ce. Unfortunately, the desired decrease in response time was never witnessed regardless of the specifics of the oxidation and reduction technique; rather, τ remained unchanged at its typical value of 100 ms at 1 W/cm^2 irradiance. As yet, we have no satisfactory explanation for this behavior, but we do believe this result may bring some further insight into the photorefractive mechanism in SBN:60/Ce.

$BaTiO_3$ crystals were also subjected to this treatment in the hope of increasing its speed. As was the case for SBN, only the two-beam coupling coefficient was affected by the oxidation and reduction process. The response time remained virtually unchanged.

Although cerium is apparently an important photorefractive species for SBN:60, the other active impurity or impurities in SBN:60 and $BaTiO_3$ remain unknown. As an attempt to discover these elements, an analysis was performed by nuclear activation of SBN:60, SBN:60/Ce, and $BaTiO_3$. Since undoped SBN:60 is photorefractive, while containing only trace quantities of cerium, we must conclude that Ce is not the only photorefractive species in SBN:60. In fact, there are significant amounts of Fe, Ni, Mo and Ta impurities present in the undoped SBN:60 crystal; Fe and Ni, for example, are known to be effective photorefractive centers in $LiNbO_3$. In $BaTiO_3$, we similarly see large quantities of Fe along with a considerable Sr content. Since strontium has not yet been directly associated with the photorefractive effect in $BaTiO_3$, we largely attribute the activity in $BaTiO_3$ to Fe. Further studies on the response of $BaTiO_3$ vs iron concentration, however, are needed to verify this claim.

3.4 Comparison of Photorefractive SBN:60, SBN:60/Ce and $BaTiO_3$

To decide if a given crystal is a useful photorefractive material, several criteria must first be defined on which to base the evaluation. The optical quality of the material is usually the property given most attention

initially. A crystal with striations, defects, or other imperfections, for example, will not find much practical use in an optical system. The optical quality of each of the three crystals we considered was excellent. Both of the SBN crystals were striation-free and their optical quality was independent of whether the crystal was poled or not. However, high optical quality in $BaTiO_3$ was only observed when the crystal was fully poled; partial depoling by a laser beam, for example, would dramatically decrease its optical clarity. Therefore, on the basis of optical quality, all three crystals were similar with the only exception that the SBN crystals are better suited for high-power laser applications.

Since the two-beam coupling coefficient Γ directly describes the magnitude of the photorefractive effect in a crystal, Γ can be reasonably used as a quantity by which to compare photorefractive materials. A crystal with a coupling coefficient less than 1 cm^{-1} is considered weakly photorefractive, while one with 1 $cm^{-1} < \Gamma < 10$ cm^{-1} is rated moderately photorefractive. Crystals whose coupling coefficients are greater than 10 cm^{-1} are labeled very photorefractive. Using these definitions as a criterion for evaluation, we see that while both SBN:60 and $BaTiO_3$ are moderately photorefractive, SBN:60/Ce, whose coupling coefficient approaches 15 cm^{-1}, is considered very photorefractive. On the basis of this criterion, therefore, SBN:60/Ce is the best photorefractive material of the three.

To use a given crystal in a high-speed optical system, its response time needs to be sufficiently short. Therefore, using τ, the photorefractive response time, we see that $BaTiO_3$ is better suited for high-speed applications than are SBN:60/Ce and SBN:60, although SBN:60/Ce is only a factor of 2 to 3 slower, and the present Ce concentration may not be optimum.

A difficulty arises when, as in our case, crystals with differing coupling coefficients and response times need to be compared. In systems using the transient response of a photorefractive material, it is possible that a slow crystal with a large Γ may exhibit higher coupling in a given unit of time than a crystal with a fast response, but small Γ. Therefore, a two-

beam coupling sensitivity S_2 is defined and given by

$$S_2 = \frac{e^{(\Gamma - \alpha)\ (1\ cm)}}{I_o \tau} \qquad (3.6)$$

Physically, S_2 describes how much coupling a given crystal of unit length will provide when irradiated with a finite amount of energy. On the basis of this criterion, we obtain the following values of two-beam coupling sensitivity for the three crystals considered:

$$S_2 \simeq 9.0 \times 10^{1}\ J^{-1} \quad (BaTiO_3)$$
$$S_2 \simeq 2.0 \times 10^{2}\ J^{-1} \quad (SBN{:}60)$$
$$S_2 \simeq 1.0 \times 10^{5}\ J^{-1} \quad (SBN{:}60/Ce)$$

Therefore, we can see both of the SBN crystals are more sensitive than $BaTiO_3$. In fact, S_2 for SBN:60/Ce is about 3 orders of magnitude larger than the corresponding value for $BaTiO_3$. Thus, in systems which rely on the transient response of a photorefractive crystal, the best candidate of the three considered here is SBN:60/Ce.

A major goal of this work has been the growth of high optical quality SBN crystals which would be more photorefractive than $BaTiO_3$. This has been accomplished by growing striation-free SBN:60 and SBN:60/Ce single crystals which can now be had as cubes approaching 1 cm on a side. When their photorefractive properties were measured, they were found to be, in most cases, substantially better photorefractive crystals than $BaTiO_3$.

4.0 GROWTH AND DIELECTRIC PROPERTIES OF ORTHORHOMBIC TUNGSTEN BRONZE CRYSTALS IN THE $Pb_{1-x}Ba_xNb_2O_6$ FAMILY

4.1 Introduction

In earlier studies, we explored the phase field beyond the morphotropic phase boundary in the region $Pb_{0.6}Ba_{0.4}Nb_2O_6$ for compositions in the tetragonal ferroelectric phase field. For these crystals, at compositions close to morphotropy, $T_{c(3)}$, the tetragonal phase Curie temperature, is slightly higher than $T_{c(1)}$, the orthorhombic ferroelectric Curie maximum. There are high values of both ε_{33} and ε_{11}, and as a result, very high values of r_{51} which persist down to room temperature. For the present study, the objective has been to explore the orthorhombic phase field gain for compositions close to morphotropy.

4.2 Phenomenology

For the orthorhomic ferroelectric forms, the nonzero components of spontaneous polarization are

$$P_1^2 = P_2^2 \neq 0, \; P_3^2 = 0 \tag{4.1}$$

and the ferroelectric species is 4/mmm(2)D2Fmm2 in the notation of Shuvalov. P_s is along the two-fold axis which makes an angle of 45° with respect to the prototypic 1 axis and lies in the 1:2 plane.

Using the Gibbs function derived earlier, it is easy to derive equations for the dielectric stiffness, spontaneous strain, piezoelectric coefficients and linear electro-optic behavior in terms of the original prototypic axes. For the dielectric stiffness, we have

$$X_{11}^T = 2\alpha_1 + 12\alpha_{11}P_1^2 + 2\alpha_{12}P_1^2 + 30\alpha_{111}P_1^4$$

$$X_{22}^T = 2\alpha_1 + 12\alpha_{11}P_1^2 + 2\alpha_{12}P_1^2 + 30\alpha_{111}P_1^4$$

$$X_{33}^T = 2\alpha_3 + 4\alpha_{13}P_1^2$$

$$X_{12}^T = 4\alpha_{12}P_1^2$$

$$X_{13} = X_{23} = 0 \ . \qquad (4.2)$$

For the spontaneous strain,

$$x_1 = (Q_{11} + Q_{12})P_1^2$$

$$x_2 = (Q_{11} + Q_{12})P_1^2$$

$$x_3 = 2Q_{13}P_1^2$$

$$x_4 = x_5 = x_6 = Q_{66}P_1P_2 = 0 \ . \qquad (4.3)$$

and piezoelectricity,

$$\begin{array}{lll} b_{11} = 2Q_{11}P_1 & b_{21} = 2Q_{12}P_1 & b_{31} = 0 \\ b_{12} = 2Q_{12}P_1 & b_{22} = 2Q_{11}P_1 & b_{32} = 0 \\ b_{13} = 2Q_{13}P_1 & b_{23} = 2Q_{13}P_1 & b_{33} = 0 \\ b_{14} = 0 & b_{24} = 0 & b_{34} = Q_{44}P_1 \\ b_{15} = 0 & b_{25} = 0 & b_{25} = Q_{44}P_1 \\ b_{16} = Q_{66}P_1 & b_{26} = Q_{66}P_1^2 & b_{36} = 0 \end{array} \qquad (4.4)$$

For the quadratic electro-optic effect,

$$\Delta B_{11} = (g_{11} + g_{21})P_1^2$$

$$\Delta B_{22} = (g_{11} + g_{21})P_1^2$$

$$\Delta B_{33} = 2g_{13}P_1^2$$

$$\Delta B_{12} = g_{66}P_1^2 \qquad (4.5)$$

and for the linear electro-optic effect,

$$r_{11} = r_{22} = 2g_{11}P_1\varepsilon_{11}$$

$$r_{12} = r_{21} = 2g_{21}P_1\varepsilon_{11}$$

$$r_{13} = r_{23} = 2g_{13}P_1\varepsilon_{33}$$

$$r_{34} = r_{35} = g_{44}P_1\varepsilon_{33}$$

$$r_{16} = r_{26} = g_{44}P_1\varepsilon_{11} \qquad (4.6)$$

Our earlier studies of the tetragonal forms close to morphotropy show that to a good approximation,

$$\alpha_1 = \alpha_{10}(T - \theta_1) \qquad (4.7)$$

and

$$\alpha_3 = \alpha_{30}(T - \theta_3) \qquad (4.8)$$

Thus, for the tetragonal ferroelectric species to occur, $\theta_3 > \theta_1$, but close to the phase boundary these became almost equal.

In the orthorhombic solution, we expect $\theta_1 > \theta_3$, but again there will be a close approach near the morphotropic composition. The consequence can then be seen in Eq. (4.2) in that

$$X_{33}^T = 2X_{30}(T - \theta_3) + 4\alpha_{13}P_1^2 \qquad (4.2b)$$

At temperatures just below θ_1 (in the ferroelectric form), T will become less than θ_3 and the first term will be negative. Since P_1^2 increases more slowly than linear below θ_1, the linearly increasing magnitude of the first negative term destabilizes the polarization and X_{33}^T becomes very small so that ε_{33} becomes large.

Turning to the electro-optic Eqs. (4.6) for very large values of ε_{33}, we may expect exceedingly large values of

$$r_{13} = r_{23} = 2g_{13}P_1\varepsilon_{33}$$

$$r_{34} = r_{35} = g_{44}P_1\varepsilon_{33}.$$

Note that since the Curie temperature is high (over 250°C), P_1, the spontaneous polarization, will be large. Also, in view of the balance of positive and negative terms in Eq. (4.2b) the temperature dependence of these very high values should be much smaller than in normal ferroelectrics where one is working close to a Curie point.

The disadvantage of the orthorhombic forms is evid from Eq. (4.3) in that through the term

$$X_6 = Q_{66}P_1P_2$$

it is evident that the spontaneous strain changes with the orientation of P_s between the four permitted domain states, i.e., the orthorhombic forms are also ferroelastic. This will have no effect once a single domain state has been achieved, but will make it more difficult to pole the crystal to the desired configuration.

In view of the potential advantage of having a very high temperature-independent transverse electro-optic effect, it appears desirable to explore the orthorhombic composition close to morphotropy. This has been the objective of our recent studies.

4.3 Crystal Growth

Single crystals of $Pb_{1-x}Ba_xNb_2O_6$ were grown by the rf-heated Czochralski technique using a CRYSTLOX MCGS3 crystal growth system. The starting compositions are specified here by the value of x in $Pb_{1-x}Ba_xNb_2O_6$ (PBN), which is obtained from the replacement of a part of Pb by Ba in $PbNb_2O_6$. The attempted values for x in this study are 0.2, 0.25, 0.3 and 0.35.

The raw materials were Specpure grade PbO, $BaCO_3$ and Nb_2O_5 supplied by Johnson-Matthey Co., England. These oxides were weighed, mixed well in the stoichiometry of PBN and ball-milled together with ethanol for 12 to 24 h in a small polyethylene container. The resulting slurry was air dried and then fired in an alumina crucible at 1050°C for 3 h. The fired product was crushed in a pestle and mortar and an excess of 10 wt% PbO was added into the crushed powder to make up for PbO volatilization during crystal growth. These powders were remixed, dried and fired at 750°C for 10 h. This procedure was adopted to ensure that the lead was in a fully oxidized state before being placed into the platinum crucible. The platinum crucible was 40 mm in both diameter and height, and was supported in an alumina crucible and covered with a platinum after-heater to reduce vertical and radial thermal gradients above the melt surface and to minimize heat losses.

Both Pt wires and $K_2BiNb_5O_{15}$ crystals were used as seed material. The crystal structures of PBN and $K_2BiNb_5O_{15}$ are of the same tungsten bronze type, although the melting point of $K_2BiNb_5O_{15}$ is lower by about 100°C. The pulling axis was chosen parallel to the a-axis to minimize cracking during growth. All growth experiments were carried out in an O_2 pressure of around 24 psi to reduce the volatilization of PbO due to the high melting point of PBN (~ 1400°C).

X-ray diffraction measurements were performed by means of a diffractometer using Ni-filtered CuKα radiation. Lattice constants a, b, and c were calculated using reflection peaks in the 2θ = 20-60° range.

4.4 Results and Discussion

Transparent, pale-yellow single crystals of PBN were grown using excess PbO to combat PbO losses due to evaporation. In spite of a large number of attempts, it was exceedingly difficult to grow large, crack-free crystals. Often, it appeared that this cracking occurred due to stresses generated by the appearance of the ferroelastic domain structure which occurs at the orthorhombic ferroelectric Curie temperature. Also, in spite of the added excess PbO and oxygen overpressure during growth, the compositions of the grown crystals differed significantly from that of the corresponding melts, as determined by the comparison of x-ray lattice spacing with that of known ceramic samples and by wet chemical analysis. The optimum PBN growth conditions are given in Table 6.

Table 6

Optimum Growth Conditions of PBN

Seed	Pt wire or $K_2BiNb_5O_{15}$
Pulling Rate	1 mm/h
Seed Rotation	20 rpm
Atmosphere	O_2 at a pressure of 24 psi
Cooling Rate	~ 50°C/h

For a PBN crystal with the composition $Pb_{0.67}Ba_{0.33}Nb_2O_6$, as revealed by chemical analysis, the Curie temperature obtained from DSC was 290°C (Fig. 15), somewhat below the value of 330°C reported in ceramic materials of the same composition. Along the 8 mm length of a crystal of this composition, DSC measurements taken from different sections along the crystal reveal a Curie point variation of less than 3°C, indicating good homogeneity.

The crystals of most interest are those at $Pb_{0.67}Ba_{0.33}Nb_2O_6$ and at the composition $Pb_{0.6}Ba_{0.4}Nb_2O_6$. The latter is very close to the reported morphotropic composition for ceramic materials, but appears to be fully in the tetragonal phase at temperatures below 225°C.

It appears from these growth runs that in every case the T_c of the single crystal is below that of the corresponding ceramic. In considering this difference, one must remember that because of the tetragonality of the high temperature bronze structure and the consequent anisotropy in thermal

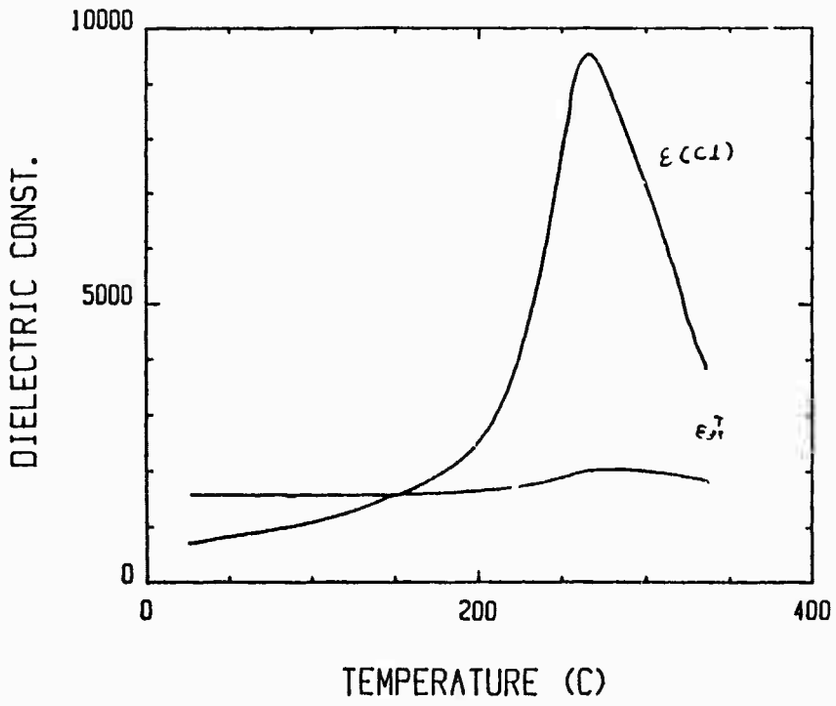

Fig. 15 Temperature dependence of T.B. $Pb_{0.67}Ba_{0.33}Nb_2O_6$ crystal.

expansion, the ceramics will not always be in a state of zero stress at T_c, so some minor difference in T_c between crystals and ceramics are to be expected.

For the two crystals very close to the morphotropic boundary, the dielectric permittivity ε_{33} and ε_{11} were measured as a function of temperature using an HP 4275A LCR meter. Sample temperature was controlled in a Delta Design environment chamber under HP 9816 computer control. The data for $Pb_{0.6}Ba_{0.4}Nb_2O_6$ is shown in Fig. 16. It is important to note the rapid increase in ε_{33} on approaching the morphotropic composition. Furthermore, as suggested by the phenomenology, these very high ε_{33} values are not strong functions of temperature in the ferroelectric phase. The reason for the apparent difference in Curie temperature for ε_{33} and ε_{11}, which is evident in both curves, is not yet understood. New measurements are now being undertaken to resolve this problem.

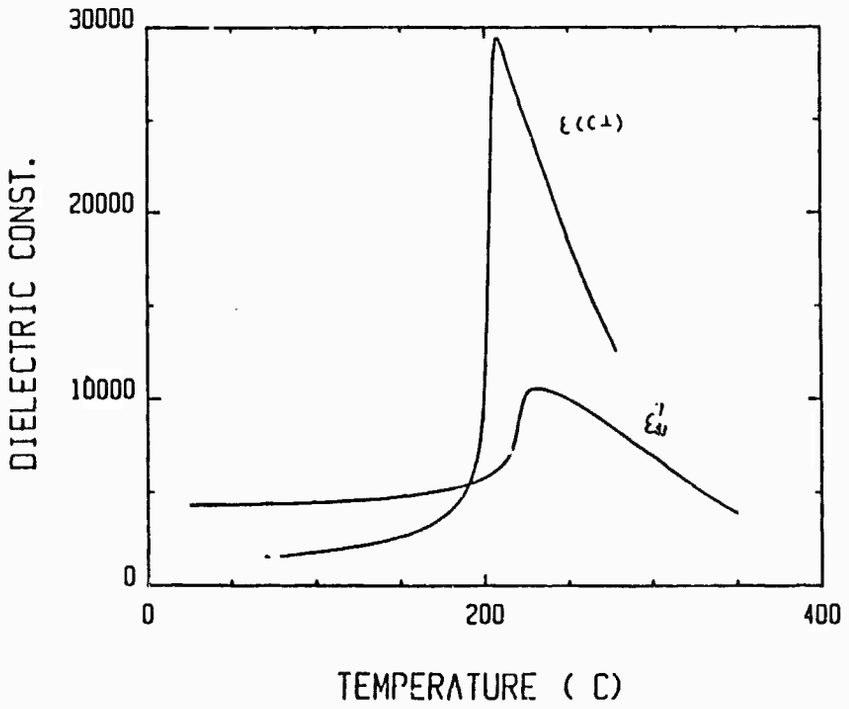

Fig. 16 Temperature dependence dielectric constant for PBN: 60 crystal.

Taking the value of g_{13} to be of order 0.09, as measured on other PBN compositions, the high P_1 and ε_{33} values lead to a predicted r_{13} value of ?000, with very little temperature dependence. Such a value is a significant improvement over $BaTiO_3$ for optical four-wave mixing and indicates the very high potential of this morphotropic bronze system for optical device applications.

5.0 EPITAXIAL GROWTH OF FERROELECTRIC TUNGSTEN BRONZE SBN FILMS

5.1 Introduction

The need for active materials for various optoelectric devices, including electro-optic,[6,7] spatial light modulators, pyroelectric detectors,[8] SAW,[9,10] and many others has stimulated recent work on the growth of ferroelectric tungsten bronze films. The bronze composition $Sr_{1-x}Ba_xNb_2O_6$, $0.75 \leq x \leq 0.25$, is very attractive and possesses electro-optic and pyroelectric coefficients higher than many other well-behaved ferroelectric materials.[11,12] Although the growth of optical quality bulk crystals of $Sr_{1-x}Ba_xNb_2O_6$ (SBN:60) has been shown to be successful,[13-16] there is great promise for other compositions within this solid solution system; hence, the LPE technique has been established for their growth. The lattice match between SBN:60 and other compositions is excellent, and SBN:60 crystals are now available for use as substrate material. The following sections report the epitaxial growth of SBN compositions using vanadium-containing flux systems for various device applications.

5.2 Experimental Procedure

The partial phase diagrams for the $M^{2+}V_2O_6$-$Sr_{1-x}Ba_xNb_2O_6$ and M^+VO_3-$Sr_{1-x}Ba_xNb_2O_6$ systems, M^{2+} = Ba or Sr, and M^+ = K, Na, Li, were established with respect to composition and temperature up to 1300°C. Reagent grade carbonates or oxides of 99.9% purity were used as starting materials for this investigation. X-ray and DTA techniques were used to identify the solid solubility range of the tungsten bronze structure, lattice constants, solidus-liquidus temperature and eutectic compositions.

$Sr_{0.6}Ba_{0.4}Nb_2O_6$ (SBN:60) single crystals were grown by the rf Czochralski technique and crystals as large as 2-3 cm in diameter and 4-6 cm long were available for use as substrate mateirals. The <001>, <100> and <110> substrates were cut from as-grown crystals and their top surfaces were optically polished. Substrate surfaces were cleaned using dilute acid and then water to remove any dust particles, oils, etc., before use in LPE film growth.

5.3 Results and Discussions

5.3.1 Solvent for Tungsten Bronze Family Compositions

Crucial to the success of isothermal LPE growth is an ability to supercool the solution without the occurrence of spontaneous nucleation. It is therefore necessary, before LPE growth is performed, to find a suitable flux system for the $Sr_{1-x}Ba_xNb_2O_6$ solid solution system. Although a large number of solvents have been identified for this family, the present work was restricted to only the vanadium-containing solvents. Based on current research on ferroelectric $LiNbO_3$ thin film growth,[17-21] it has been found that the vanadium-containing solvents are useful for SBN and the bronze compositions because of the following important reasons:

1. V^{5+} cation has a strong preference for the four-fold coordinated site, and hence, no vanadium inclusion in the bronze film is expected.

2. Supercooling range for the V^{5+}-containing solvents is reasonably high, on the order of 20-30°C.

3. V^{5+}-containing solvents melt at significantly low temperature and thus allow LPE growth at much lower temperatures.

4. V^{5+}-containing solvents are remarkably stable at elevated temperatures (up to 1100°C).

5. All V^{5+}-containing solvents dissolve in dilute acids.

Table 7 summarizes a number of flux systems used in the present study for the SBN solid solution system. Since this system contains five or more components, the determination of a complete phase diagram is impractical. As

Table 7

Flux Systems for Tungsten Bronze Compositions

SYSTEM	MELTING TEMPERATURE OF FLUX (° C)	EUTECTIC TEMPERATURE (° C)*	MAIN PHASE	REMARKS
BaV_2O_6 - $Sr_{1-x}Ba_xNb_2O_6$	720	685	$Sr_{1-x}Ba_xNb_2O_6$ ($0.46 \leq x \leq 0.38$)	Useful range for LPE work
BaB_8O_{13} - $Sr_{1-x}Ba_xNb_2O_6$	890	800	$Sr_{1-x}Ba_xNb_2O_6$	Useful range for LPE work
SrV_2O_6 - $Sr_{1-x}Ba_xNb_2O_6$	760	710	$SrNb_2O_6$	Not suitable
KVO_3 - $Sr_{1-x}Ba_xNb_2O_6$	520	490	$Sr_2KNb_5O_{15}$ **	Useful range for LPE work
$NaVO_3$ - $Sr_{1-x}Ba_xNb_2O_6$	630	570	$Sr_2NaNb_5O_{15}$	Useful range for LPE work
$LiVO_3$ - $Sr_{1-x}Ba_xNb_2O_6$	700	680	$LiNbO_3$ + $Sr_{1-x}Ba_x$-Nb_2O_6	Not suitable
Li_2WO_4 - $Sr_{1-x}Ba_xNb_2O_6$	920	850	$LiNbO_3$	Not suitable

* = Phase relation was studied up to 1300°C

** = Belongs to Tungsten Bronze Family

described by Roy and White,[22] such systems can be treated as pseudo-binary with the phase to be crystallized as one component (solute) and the flux (solvent) as the other. Using this concept, as summarized in Table 7, several flux systems were investigated for the SBN solid solution system.

The determination of the phase diagrams BaV_2O_6-$Sr_{1-x}Ba_xNb_2O_6$ and BaB_8O_{13}-$Sr_{1-x}Ba_xNb_2O_6$, as shown in Fig. 17, indicate that the ferroelectric tetragonal SBN phase exists over a wide range of temperature and compositional conditions. X-ray measurements on these systems indicated that the crystallized compositions are Ba^{2+}-rich with $0.54 \leq x \leq 0.62$. In the third system, SrV_2O_6-$Sr_{1-x}Ba_xNb_2O_6$, $SrNb_2O_6$ was a major phase and extended over a wide compositional range. This system was found to be unsuitable for bronze compositions. In two other systems, KVO_3-$Sr_{1-x}Ba_xNb_2O_6$ and $NaVO_3$-$Sr_{1-x}Ba_xNb_2O_6$, although the tungsten phases crystallized over a wide compositional range, the composition of the phases in each system was different, e.g., $Sr_2KNb_5O_{15}$ (tetragonal) and $Sr_2NaNb_5O_{15}$ (orthorhombic) in the respective systems.[23,24] Since compositions from both systems exhibit excellent dielectric, pyroelectric and electro-optic properties, these systems will be considered for future growth work.

The remaining two flux systems, $LiVO_3$-$Sr_{1-x}Ba_xNb_2O_6$ and Li_2WO_4-$Sr_{1-x}Ba_xNb_2O_6$ (nonvanadium system), did not produce tungsten bronze compositions of SBN until 75 mole% or more of $Sr_{1-x}Ba_xNb_2O_6$ was in the mixture, and would require a dipping temperature of at least 1300°C. $LiNbO_3$ was found to be a more stable phase in these systems instead of bronze SBN.

Since the $Sr_{1-x}Ba_xNb_2O_6$ solid solution is stable in only two systems, BaV_2O_6-SBN and BaB_8O_{13}-SBN, the choice of solvents is very limited. Furthermore, since the tetragonal ferroelectric phase exists over a wide compositional range for $Sr_{1-x}Ba_xNb_2O_6$, $0.75 \leq x \leq 0.25$, it is important to establish the Sr:Ba ratio in each composition before any film growth experiments are conducted.

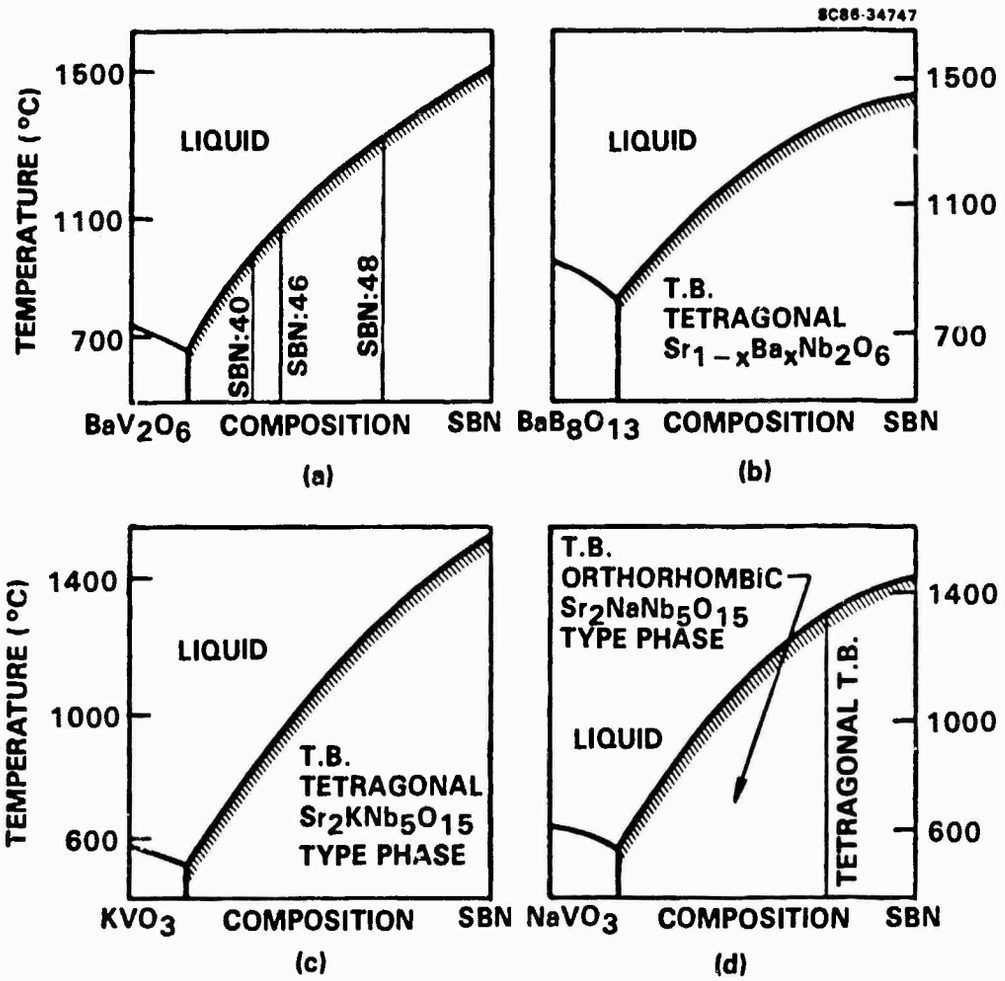

Fig. 17 Partial phase diagram for $M^{2+}V_2O_6$-SBN and $M^{+}VO_3$-SBN systems.

The BaV_2O_6-SBN system was considered in this work. This system was further modified as the ternary system BaV_2O_6-$SrNb_2O_6$-$BaNb_2O_6$. Figure 18 shows the structural stability of various phases, including tungsten bronze $Sr_{1-x}Ba_xNb_2O_6$, $0.75 \leq x \leq 0.25$. Since SBN is a solid solution system, the Sr:Ba ratio must be established to check lattice compatibility with SBN:60 substrates. For this reason, we studied the joint BaV_2O_6-$Sr_{0.5}Ba_{0.5}Nb_2O_6$ using x-ray diffraction and DTA techniques. Based on lattice constant measurements, the compositions along this line are predominantly Ba^{2+}-rich and varied from $Sr_{0.4}Ba_{0.6}Nb_2O_6$ (SBN:40) to $Sr_{0.46}Ba_{0.54}Nb_2O_6$ (SBN:46) with increasing SBN:50 concentration in the system. The DTA results indicate that a pseudo-eutectic occurs at 15 mole% of SBN:50, with a eutectic temperature of ~ 685°C. The supercooling range for this system is reasonably large at an estimated 25°C, which is suitable for film growth experiments.

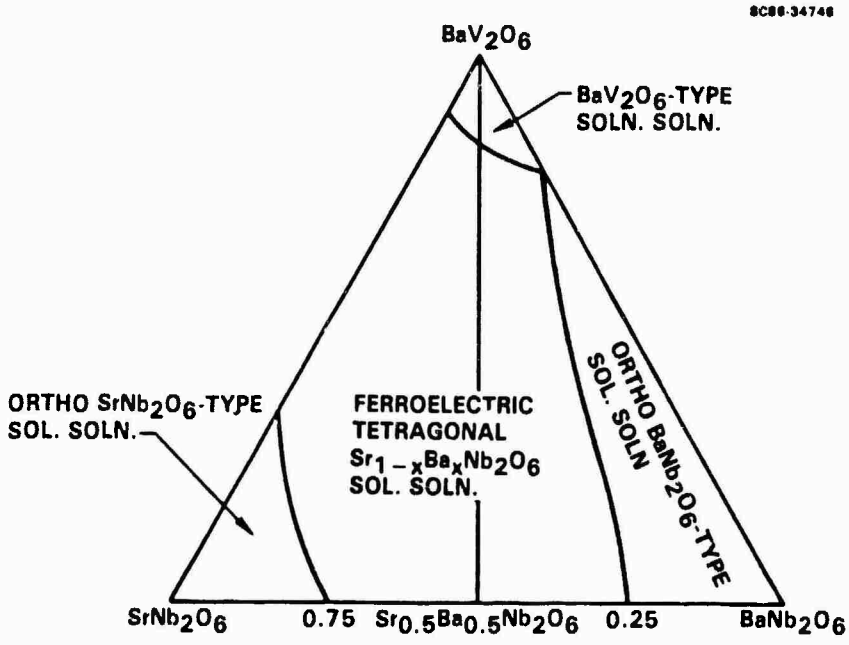

Fig. 18 System BaV_2O_6-$SrNb_2O_6$-$BaNb_2O_6$-SBN in air at 1300°C.

5.3.2 LPE Growth of SBN Thin Films

The compositions SBN:40 and SBN:46, which correspond to the batch mixtures 60 mole% BaV_2O_6-40 mole% SBN:50 and 70 mole% BaV_2O_6-30 mole% SBN:50, respectively, were selected for epitaxial growth studies. The lattice constants, ferroelectric properties and electro-optic properties for these SBN compositions and for $LiNbO_3$ are given in Table 8. An important consideration for the growth of SBN:40 and SBN:46 on SBN:60 substrates is a sufficiently close lattice match between films and substrate; as given in Table 8, the lattice match for these compositions with SBN:60 is fairly close, on the order of 0.6% or less on the <100> and 0.3% or less on the <100> or <110> oriented faces.

Initially, efforts concentrated on the growth of the SBN:46 composition, since it has a closer lattice match to SBN:60. The calcined mixture was melted in a 100 cc platinum crucible and then placed in the growth furnace as shown in Fig. 19. The growth apparatus consists of a vertical tube furnace whose temperature was controlled with an accuracy of ±1°C. The mixture was held overnight at ~ 100°C above its melting temperature, and after achieving complete homogeneity, the molten solution was slowly cooled to the growth temperature at the rate of 10°C/h. An oriented SBN:60 substrate, positioned slightly above the melt in order to equilibriate with the solution temperature was then dipped into the melt. Table 8 summarizes the substrate orientations, dipping temperature range, lattice constants and film compositions.

After the required growth time had elapsed, the sample was withdrawn from the melt and cooled very slowly to room temperature. The adhering flux was removed by dipping the film/substrate in dilute HCl acid. This is the first time such ferroelectric SBN films have been grown by this technique; however, the growth of other tetragonal bronze compositions by sputtering and LPE techniques has also been reported.[25,26]

Table 8

Structural and Optical Properties of Bronze Compositions

MATERIAL	$Sr_{0.6}Ba_{0.4}Nb_2O_6$ (SBN:60)	$Sr_{0.46}Ba_{0.54}Nb_2O_6$ (SBN:46)	$Sr_{0.48}Ba_{0.6}Nb_2O_6$ (SBN:40)	$LiNbO_3$
LATTICE CONSTANTS	a = 12.462 Å c = 3.938 Å	a = 12.473 Å c = 3.953 Å	a = 12.478 Å c = 3.958 Å	a = 5.148 Å c = 13.784 Å
LATTICE MISMATCH*		[001] = 0.38% [100] = 0.13% [110] = 0.20%	[001] = 0.52% [100] = 0.16% [110] = 0.19%	
LPE GROWTH TEMP (°C)		1040° to 1050°	920° to 930°	
GROWTH RATE (m/Min.)		[001] = 1 to 2 µm [100] = 0.5 µm [110] = 0.5 µm	[001] = 1 to 2 µm [100] = 0.5 µm [110] = 0.5 µm	
Tc (°C)	78°	135°	160°	1150°
ELECTRO-OPTIC COEFF. xLO^{-12} m/V	r_{33} = 420 r_{13} = 60	r_{33} = 180 r_{13} = 35	r_{33} = 110 r_{13} = 25	r_{33} = 30 r_{13} = 8.6
SAW COUPLING CONSTANT	[001] = 180 x 10^{-4}	[001] = 100 x 10^{-4}	------	[100] = 420 x 10^{-4}
POLING FILED	[001] = 7 kV/Cm [100] = 10 kV/Cm [110] = 10 kV/Cm	[001] = 8 kV/Cm. [100] = 10 kV/Cm. [110] = 10 kV/Cm.	[001] = 8 kV/Cm. [100] = 10 kV/Cm. [110] = 10 kV/Cm.	

* → With respect to SBN:60

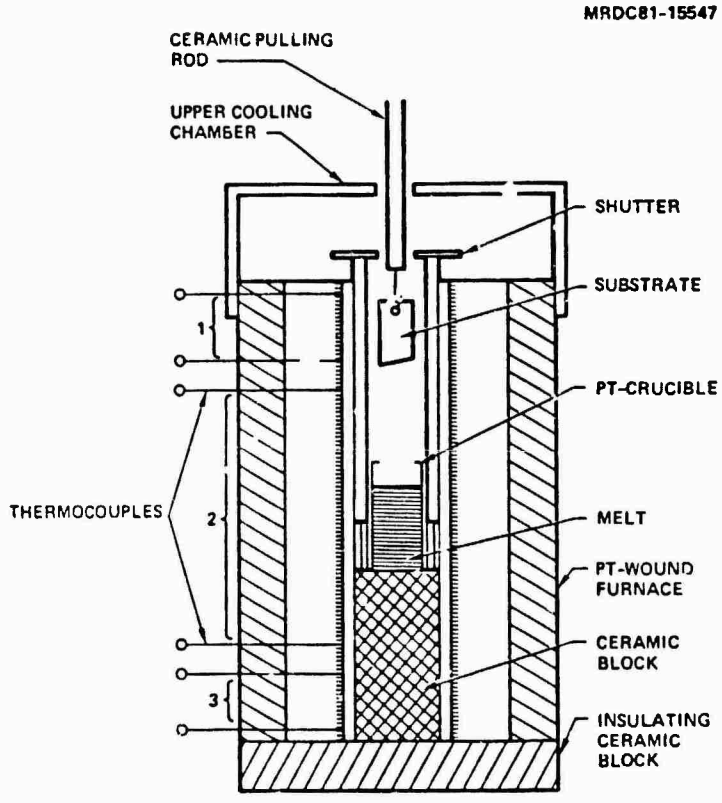

Fig. 19 Diagram of furnace for LPE.

The success of thin film growth is due, in part, to the availability of large, high quality SBN:60 substates. Since SBN:60 bulk crystals exhibit 24 well-defined facets, the maintenance of precise substrate orientations was a relatively easy task. The films were developed on three different orientations, spcifically, <001>, <100> and <110>, and the LPE growth process was studied with respect to growth temperature, orientation and lattice match. It was found that the film quality and thickness depend strongly on the substrate orientation and the rate of crystallization. For example, growth was ~ 3-4 times faster on the <001> direction as compared to the <100> and <110> directions. This is consistent with our observations on bulk single crystal growth

of SBN compositions by the Czochralski technique, where the growth rate is considerably greater along the <001> direction, whereas growth along other orientations has been found to most difficult and, in some instances, impossible.

Figure 20 shows a typical cross section for a thin film grown on a <001>-oriented SBN:60 substrate. The growth rate was typically 1-2 μm/min on the <100> direction, while under the same conditions, the rate was less than 0.5 μm/min or less on the <100> and <110> directions. However, because of the lower growth rates on the latter directions, the film quality was superior and films as thick as 5-25 μm were grown without compromising quality or ferroelectric properties.

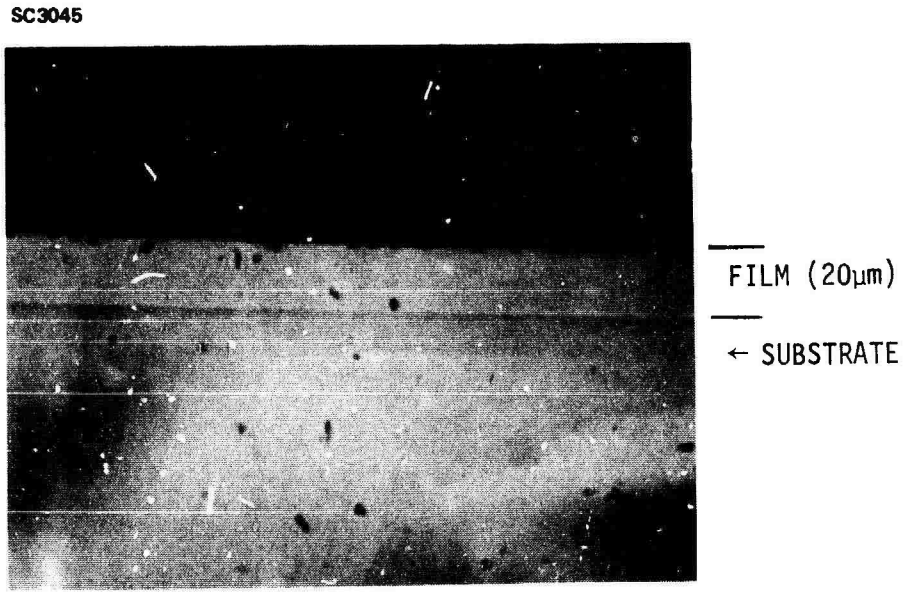

Fig. 20 Cross section of 20 m SBN:46 film on (001)-oriented SBN:60 substrate.

The quality of the <001>-oriented films was studied with respect to growth temperature for both batch mixtures, and was found to improve considerably with an increase in growth temperature from 1040-1050°C and 930-940°C, respectively. However, the film quality gradually degraded for the composition corresponding to SBN:40 (Batch 1), probably because of the increased lattice mismatch for <001> oriented films. These films also showed a tendency to crack. However, for the <100> and <110> oriented substrates, film quality was excellent for both mixtures.

Although the tetragonal $Sr_{1-x}Ba_xNb_2O_6$ solid solution extends over a wide compositional range, the change in the c lattice constant is more pronounced as compared with the change in a. Our results suggest that for the successful epitaxial growth of these bronze compositions, it is important to maintain a 0.3% or less lattice match between the film and substrate along the growth direction. Recent work by Adach et al[26] also demonstrated the growth of excellent quality bronze $K_3Li_2Nb_5O_{15}$ films on $K_2BiNb_5O_{15}$ substrates using the LPE and sputtering techniques. Clearly, to generalize these results, further work is necessary to establish the tolerance factors for allowable lattice mismatch in the growth of bronze composition films.

5.3.3 Characterization

In order to confirm single phase film growth and to accurately determine composition, the a and c lattice constants for both film and substrate were measured using the x-ray diffraction technique. Figure 21 shows x-ray reflections for films grown from the batch mixture 60 mole% BaV_2O_6-40 mole% SBN:50. The composition for the film was established by measuring the difference between the substrate and film lattice constants. This technique was previously used with success in our work to establish the dopant concentration in $LiNbO_3$ films.[17,18] As shown in Fig. 21, two reflections corresponding to <003> and <004> for the c axis, and <10,00> and <12,00> for the a axis were studied for both film and substrate. Since changes for the a axis are small as compared to the c axis, it was necessary to select higher angle reflections to get adequate separation between the film and substrate peaks. Using these

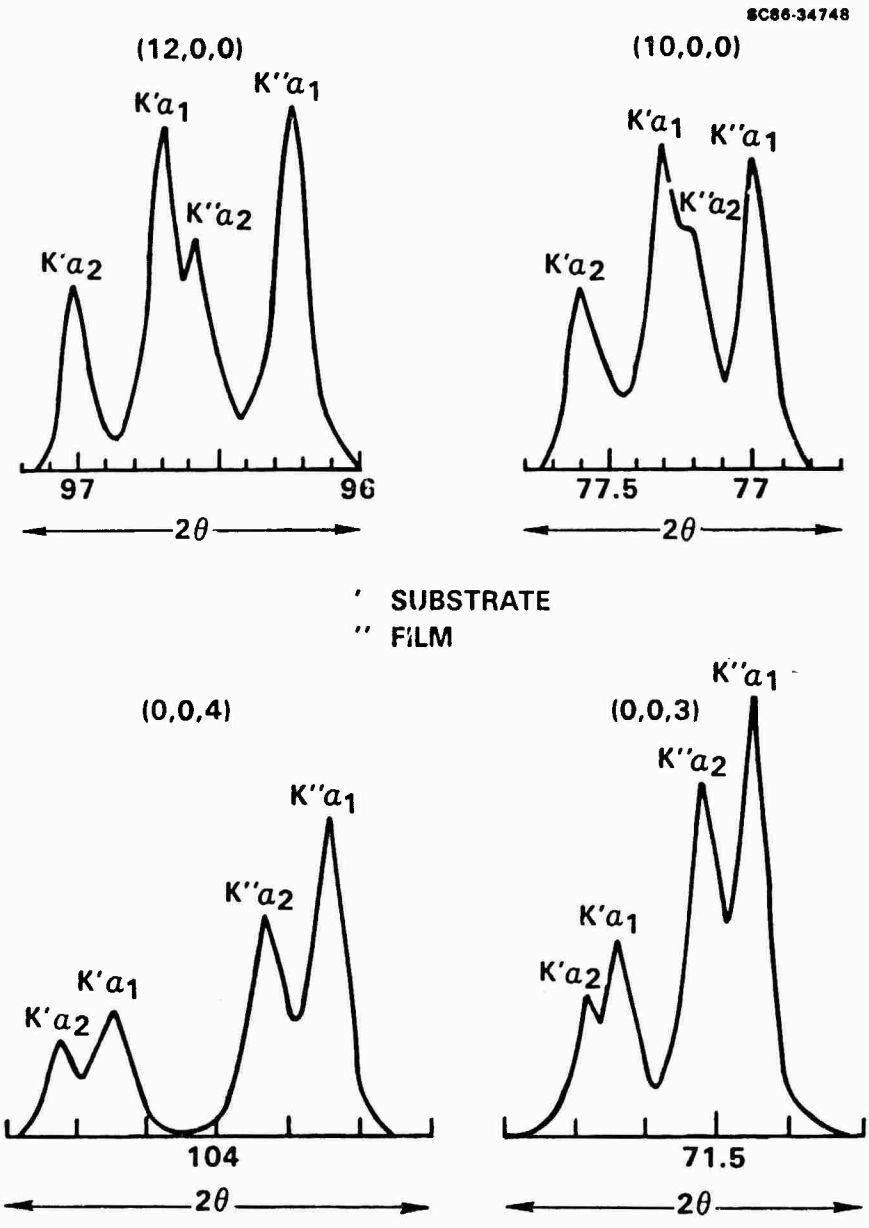

Fig. 21 X-ray diffraction peaks for SBN film/substrate.

reflection values, the lattice constants a and c were determined for both film compositions, and they are as follows:

SBN:46	a = 12.476Å	c = 3.956Å
SBN:40	a = 12.482Å	c = 3.961Å

These films exhibited unchanging lattice parameters with variations of growth process parameters until the vanadium loss due to volatilization became significant. These constants are reasonably close to the values reported for SBN:46 and SBN:40 in Table 8 and, based on these results, it seems that the growth of uniform compositions is possible. It is also clear from these experiments that the films are Ba^{2+}-rich over a wide range of compositions in the BaV_2O_6-SBN:50 system. At higher concentrations of Sr^{2+}, the major phase formed is nonferroelectric $SrNb_2O_6$, which is of no interest in this work.

The SAW electro-mechanical coupling constant (K^2) for SBN:46 films was measured on poled (001)-plates propagating the <100> direction using the method described by Staples.[27] The films were poled in all configurations, but it was found that the poling of <100> and <110>-oriented films was more difficult as compared to films grown on the <001> direction. Although the quality of the <001>-oriented films is not as good as that achieved for the other orientations, it was still possible to evaluate the coupling constant for these films. The coupling constant for SBN:46 is $\sim 100 \times 10^{-4}$, which is smaller than the current best SBN:60 bulk crystals, 180×10^{-4}. These films were also tested for optical waveguide applications using a He-Ne laser operating at 6328Å, and it was found that the quality of the <100> and <110> films is quite reasonable, whereas the <001>-oriented films were found to be unsuitable. Although the electro-optic (r_{33}) and pyroelectric coefficients for SBN:46 are not as large for SBN:60, r_{33} is at least five times better than for current $LiNbO_3$ crystals. The composition SBN:50 is now being studied in our laboratory for pyroelectric detection because of its excellent pyroelectric figure-of-merit. It is, therefore, expected that the development of better quality films have a significant impact on ongoing research programs in optical waveguides and pyroelectric thermal detectors.

6.0 FUTURE PLANNED WORK

1. Establish the optimum cerium concentration in SBN:60 crystals to obtain a 10 ms response time. Modify the growth technique accordingly.

2. Continue the development of Fe- and Cr-doped SBN:60 and attempt to establish the dopant valence states using optical spectroscopy and other analytical techniques.

3. Establish the Czochralski growth technique for La^{3+}-doped SBN:50 crystals to obtain ~ 2 cm diameter crystals for pyroelectric detector study. Also investigate the role of other cations such as Ca^{2+} and Y^{3+} in SBN:50 for pyroelectric detector applications.

4. Continue to evaluate photorefractive properties, specifically charge density, speed and sensitivity, with respect to dopants in SBN:60 using two- and four-wave mixing techniques.

5. Continue measurement of the electro-optic coefficients r_{33}, r_{51}, etc., for near-morphotropic single crystal PBN compositions.

6. Develop suitable flux systems for tungsten bronze $Sr_2KNb_5O_{15}$ LPE growth.

7. Determine the phase relation with respect to temperature and composition for various MPB compositions to establish crystal growth data.

7.0 PUBLICATIONS AND PRESENTATIONS

7.1 Publications

1. R.R. Neurgaonkar and W.K. Cory, "Progress in Photorefractive Tungsten Bronze Crystals," J. Opt. Soc. Am. B 3(2), 274 (1986).

2. R.R. Neurgaonkar, W.K. Cory and J.R. Oliver, "Growth and Applications of Tungsten Bronze Family Crystals," SPIE Southwest Conf. on Optics, Vol. 540, 146 (1985).

3. R.R. Neurgaonkar and L.E. Cross, "Piezoelectric Tungsten Bronze Crystals for SAW Applications," in preparation.

4. R.R. Neurgaonkar, W.K. Cory and J.R. Oliver, "Growth of Tungsten Bronze KLN Crystals," submitted to the J. Cryst. Growth.

5. R.R. Neurgaonkar and E.T. Wu, "Growth of Ferroelectric Tungsten Bronze SBN Thin Films by the LPE Technique," in preparation.

6. L.E. Cross and R.R. Neurgaonkar, "A Phenomenological Analysis of Tungsten Bronze Ferroelectrics," submitted to Mat. Science.

7. O. Eknoyan, C.H. Bulmer, H.F. Taylor, W.K. Burns, A.S. Greenblatt, L.A. Beach and R.R. Neurgaonkar, "Vapor Diffused Optical Waveguides in Strontium Barium Niobate (SBN:60)," Appl. Phys. Lett. 48, 13 (1986).

8. C.H. Bulmer, O. Eknoyan, H.F. Taylor, A.S. Greenblatt, L.A. Beach and R.R. Neurgaonkar, "Formation and Properties of Optical Waveguides in Strontium Barium Niobate," accepted for publication in "Processing of Guided-Wave Optoelectronic Materials-2," SPIE, Los Angeles (1986).

9. G. Rakuljic, A. Yariv and R.R. Neurgaonkar, "Photorefractive Properties of Undoped and Doped Single Crystal SBN:60," SPIE, Los Angeles (1986).

10. G. Rakuljic, A. Yariv and R.R. Neurgaonkar, "Ce-doped SBN:60 Crystals for Phase Conjugate Optics," accepted for publication in Appl. Phys. Lett.

11. E.J. Sharp, M.J. Miller, G.L Wood, W.W. Clark, G. Salamo and R.R. Neurgaonkar, "SBN as a Broadband Self-Pumped Phase Conjugate Mirror," submitted to Ferroelectrics Journal.

7.2 Presentations

1. R.R. Neurgaonkar, J.R. Oliver and E.T. Wu, "Epitaxial Growth of Ferroelectric Films," presented at the 6th Intl. Conf. on Ferroelectricity, Koboe, Japan (1985).

2. R.R. Neurgaonkar, W.K. Cory and J.R. Oliver, "Growth and Applications of Tungsten Bronze Family Crystals for Optical Applications," presented at the SPIE Optical Meeting, San Diego, CA (1985).

3. R.R. Neurgaonkar and W.K. Cory, "Ferroelectric Tungsten Bronze Crystals for Photorefractive Applications," presented at the Materials Research Soc. Symp. on Nonlinear Optical Materials, Boston, MA (1985).

4. M.D. Ewbank, R.R. Neurgaonkar, W.K. Cory and J. Feinberg, "Photorefractive Properties of SBN:60," presented at the Materials Research Soc. Symp. on Nonlinear Optical Materials, Boston, MA (1985).

8.0 REFERENCES

1. K. Megumi and H. Furuhata, J. Mat. Science 11, 1583 (1976).

2. S.T. Liu and R.B. Maciolek, J. Electronics Mat. 4, 91 (1975).

3. F.W. Ainger, W.P. Bickley and G.V. Smith, Proc. Brit. Ceram. Soc. 18, 221 (1970).

4. T. Ikeda, K. no, K. Oyamada, A. Sagara, J. Kato and S. Takano, Jap. J. Appl. Phys. 17, 341 (1978).

5. L.E. Cross and R.R. Neurgaonkar, submitted to J. Mat. Science.

6. R.R. Neurgaonkar, W.K. Cory and J.R. Oliver, Ferroelectrics 15, 3 (1983).

7. R.R. Neurgaonkar, J.R. Oliver and L.E. Cross, Ferroelectrics 56, 31 (1984).

8. A.M. Glass, J. Appl. Phys. 40, 4699 (1969).

9. R.R. Neurgaonkar and L.E. Cross, submitted to Mat. Res. Bull.

10. P.V. Lanzo, E.G. Spencser and A.A. Ballman, Appl. Phys. Lett. 11, 23 (1967).

11. J.B. Thaxter, Appl. Lett. 15, 210 (1969).

12. R.R. Neurgaonkar, M.H. Kalisher, T.C. Lim, E.J. Staples and K.K. Keester, Mat. Res. Bull. 15, 1235 (1980).

13. R.R. Neurgaonkar and W.K. Cory, J. Opt. Soc. Am. 3(2), 232 (1986).

14. R.R. Neurgaonkar, Proc. of SPIE 465, 97 (1984).

15. R.R. Neurgaonkar, T.C. Lim, E.J. Staples and L.E. Cross, IEEE Proc. of Ultrasonic Symp., 410 (1980).

16. R.R. Neurgaonkar, M.H. Kalisher, E.J. Staples and T.C. Lim, Appl. Phys. Lett. 35(8), 606 (1979).

17. E.J. Staples, R.R. Neurgaonkar and T.C. Lim, Appl. Phys. Lett. 32, 197 (1978).

18. A. Baudrant, H. Vial and J. Daval, Mat. Res. Bull. 10, 1373 (1975).

19. R.R. Neugaonkar and E.J. Staples, J. Cryst. Growth 54, 572 (1981).

20. R.R. Neugaonkar, Semi-Annual Tech. Report No. 4, Contract N00014-82-C-2466.

21. R. Roy and W.B. White, J. Cryst. Growth 33, 314 (1968).

22. G. Burns, E.A. Giess, D.F. O'Kane, B.A. Scott and S.W. Smith, J. Phys. Soc. Jap. 28, 153 (1970).

23. W. Smith, J. Phys. Soc. Jap. 28, 153 (1970).

24. T. Ohta and R.A. Watanate, Jap. J. Appl. Phys. 9, 721 (1970).

25. M. Adachi, T. Shiosaki and A. Kawabata, Jap. J. Appl. Phys. 18, 1637 (1979).

26. M. Adachi, M. Hori, T. Shiosaki and A. Kawabata, Jap. J. Appl. Phys. 17, 2053 (1978).

27. E.J. Staples, Proc. of the 28th Annual Frequency Control Symp., 280 (1974).